

サヘルの降水量を増加に転じさせた  
全球気候シフトの診断

平成 20 年 度

三重大学大学院生物資源学研究科  
博士前期課程 共生環境学専攻

宗 本 政 紀

平成 20 年度 修士論文

サヘルの降水量を増加に転じさせた  
全球気候シフトの診断

**The recent increasing trend of the precipitation in Sahel  
and its associated interhemispheric dipole of the global SST**

三重大学大学院生物資源学研究科  
共生環境学専攻 自然環境システム学講座  
地球環境気候学研究室

507M237 宗本 政紀  
指導教員 立花義裕教授

平成 21 年 3 月 3 日

## **Abstract**

The Sahel region, located in the southern of the Sahara desert underwent an unprecedented severe drought involved with the decrease of the precipitation in 1970s and 1980s. However, since the middle of 1980s the annual mean precipitation in Sahel has gradually increased. This trend shift signifies the occurrence of a global climate shift. This study diagnoses the relation of the trend shift in Sahel with global atmospheric fields and Sea Surface Temperature (SST). The present study clarifies that the shift of the precipitation trend occurred not only within Sahel but also all over the world. Significant precipitation-shifted areas are in South America, northern Eurasia and Australia. The precipitation variability in Sahel is remarkably similar to the north-south SST polarity that is the SST contrast between the area-averaged SST in the Southern Hemisphere and in the Northern Hemisphere. When the SST in the Southern Hemisphere was colder than that of the Northern Hemisphere, the precipitation in Sahel was larger than normal. In addition, this north-south interhemispheric contrast of the global SST has remarkably similar trend to that of Sahel precipitation. The trend of the SST contrast is also in association with the trends of global-scale meridional and zonal atmospheric circulations. In years of the increasing trend of the Sahel precipitation, an updraft strengthened over North Africa along with the increase of the specific humidity. These results suggest that the SST contrast determined the precipitation trends on the earth through the change of the global atmospheric circulations.

## 1. Introduction

The Sahel region, located along the southern fringe of the great Sahara desert, is the semi-arid zone and experiences a hot, desert climate for most of the year and a tropical, rainy climate for the rest [Griffiths 1972]. In this region it rains from June through September derived from Inter-tropical Convergence Zone (ITCZ) and the percentage of the precipitation during this period is about 90% of the annual precipitation. Land degradation in arid lands is now recognized as one of the most important environmental problems for the 21<sup>st</sup> century and Sahel is often quoted as the most seriously affected region [Hountondji et al. 2006, Thiaw and Mo 2005]. This region underwent an unprecedented severe drought involved with the decrease of the precipitation in 1970s and 1980s [Omotosho 2008, Heumann et al. 2007, Nicholson and Webster 2007, Hountondji et al. 2006, Giannini et al. 2003]. Hoerling et al. [2006], moreover, showed that the 1950-99 time histories of northern Africa rainfall during their respective wet seasons were well described by linear downward trends. Owing to this decreasing precipitation, many people and livestock have starved to death.

However, since 1990s the precipitation in West Africa including Sahel seems to have been gradually increasing [Folts and McPhaden 2008, Hagos and Cook 2008, Omotosho 2008, Heumann et al. 2007, Fall et al. 2006, Hountondji et al. 2006]. Hoerling et al. [2006] also emphasized that Sahel might experience a recovery in rainfall from a low point in the 1980s to values that consistently exceed the 1950-99 climatology after 2000, and this rainfall increasing is physically consistent with a projected warming of the North Atlantic Ocean compared with the South Atlantic. These situations imply that some kinds of regional or global climate shifts induced the precipitation change over Sahel. Nevertheless, no clear explanation concerned with the relation between the recent precipitation increasing and global climate shifts has been executed yet.

Only a few previous studies adverted to the climate and SST variability for the recent increasing precipitation [Folts and McPhaden 2008, Hagos and Cook 2008, Hoerling et al. 2006]. Hagos and Cook [2008] emphasized that the primary cause of the 1980s Sahel drought is divergent flow in lower troposphere associated anomalous anticyclonic circulation. This condition is related to Indian Ocean warming and concurrent tropical Atlantic warming. Additionally their model simulations showed partial recovery of the precipitation in the 1990s is mainly related to the warming of the northern tropical Atlantic Ocean and an associated cyclonic circulation that supplies the Sahel with moisture. Hoerling et al. [2006] emphasized that drying over Sahel during boreal summer is a response to warming of the South Atlantic relative to North Atlantic SST, with the ensuing anomalous interhemispheric SST contrast favoring a more southern position of the Atlantic intertropical convergence zone. Folland et al. [1986] demonstrated that persistently dry and wet periods over the Sahel region were accompanied by an interhemispheric contrast in SST; drought (pluvial) periods are linked to warm (cold) SSTs in the Southern Hemisphere relative to those of the Northern Hemisphere. Furthermore Giannini et al. [2003] emphasized that a positive trend in equatorial Indian and southern Atlantic SST were identified as the cause for the negative rainfall trend observed in Sahel from the late 1960s to the 1980s.

These studies tried to interpret the long-term or short-term variability of the precipitation in Sahel from various aspects. However most studies focused only on the rainy season in Sahel and were limited within the relationship between precipitation variability during rainy season and the SST surrounding Africa or atmospheric circulations only around Africa. Indeed, Folland et al. [1986] showed the relationship with a northern and southern hemispheric contrast of global SST, no studies on the relationship between the recovery of the rainfall in Sahel and the global SST have been

executed yet.

The present study diagnoses the physical process of the trend shifts of interhemispheric global climate and interhemispheric concurrent SST involved with the recent increasing trend of the precipitation in Sahel.

## **2. Data**

The precipitation data employed in this study is Global Precipitation Climatology Centre (GPCC), which is the global analysis of monthly precipitation on earth's landsurface based on in situ raingauge data. We use the Full Data Reanalysis Product, which is based on all stations, near real-time and non real-time, in the GPCC data base. The data covers the period from 1901 to 2007 and the spatial resolution is 0.5-degree latitude and 0.5-degree longitude global grid [Schneider et al. 2008]. The present study analyzed the data from 1959 through 2007, in which the terms of the sever drought in Sahel (1981-1985) is included.

We also use National Centers for Environmental Prediction / National Center for Atmospheric Research (NCEP / NCAR) Reanalysis data products [Kalnay et al. 1996] in order to diagnose the presence of the climate shift in inter-hemispheric global atmosphere. The SST data we use is National Oceanic and Atmospheric Administration / the extended reconstructed sea surface temperature version 3 (NOAA ERSST V3), which is constructed using the recently available International Comprehensive Ocean-Atmosphere Data Set (ICOADS) SST data and improved statistical methods that allow stable reconstruction using sparse data [Smith et al. 2007, Xue et al. 2003]. The spatial resolution of this SST data is 2.0-degree latitude and 2.0-degree longitude global grid. Both NCEP Reanalysis data and NOAA ERSST V3 we use are provided by the

NOAA/OAR/ESRL PSD, Boulder, Colorado, USA, from their Web site at <http://www.cdc.noaa.gov/>. The analysis period for NCEP / NCAR Reanalysis data and ERSST V3 is also 1959 through 2007.

### **3. Methods**

The definition of the Sahel region in this study is as follows. The region in which annual mean precipitation is from 100 to 500 mm/year within the area to the west of 20° E. The area is indicated in Figure 1. The interannual variation of the area-averaged annual mean precipitation in the Sahel region is shown in Figure 2. The minimum was in 1984. It is obvious that the precipitation has a declining trend before 1984, whereas an increasing trend after 1984. We thus regard the year of 1984 as the turning point of the precipitation trend. Henceforward, we divide analysis years into two sub-periods; one is before 1984 and the other is after 1984. A linear trend in each sub-period is also superimposed in Figure 2. By using the interannual time series and the trend in each sub-period, we will calculate the remote relationship of the precipitation in other regions on the earth, large-scale atmospheric fields and SSTs with the Sahel precipitation. All the atmospheric fields, the SST and the precipitation analyzed in this study are annual mean values. The atmospheric fields we analyzed are the geopotential height, the wind strength and direction, the velocity potential, streamfunction, the specific humidity, thickness, and the atmospheric stability. Especially, the differences of the trends in the atmospheric and oceanic fields are to be emphasized in this study in order to make the contrast clear between the sub-period before and after 1984.

## **4. Results**

### **4.1 Precipitation trend shift**

As shown in Figure 2, a large shift of the precipitation trend occurred in 1984. In addition to the precipitation variability within Sahel, the global precipitation trends before 1984 and after 1984 are demonstrated in Figure 3. The region in which the precipitation trends shifted as of 1984 is again confirmed in the region of the Northern Africa including Sahel. In addition, it should be noted that the shift of the precipitation trend occurred not only in Sahel but also over the various areas on earth. For example the northern part of the Eurasia experienced the same shift as in Sahel, i.e., before 1984 this area underwent decreasing trend of the precipitation, while after 1984 it was increasing trend. In contrast, the central region of South America and Australia show a reversed trend shift. The overall shift in the pan-Eurasian area along with Africa is in phase, whereas the shift in the Pan-American area along with Australia is overall out-of-phase to the pan-Eurasia.

### **4.2 The horizontal structure of the climate shifts**

The precipitation trend shift in many areas on the earth implies the occurrence of the trend shift in global-scale atmospheric circulations. The trend of the annual mean geopotential height and wind at the 200hPa, 600hPa, and 1000hPa before and after 1984 are shown in Figures 4, 5, and 6. Before 1984 the lower and middle troposphere over the whole area of Africa and southern Eurasia experienced the strengthening of a high-pressure trend, in contrast, areas around South Pole experienced the strengthening of a low-pressure trend (Figures 5 and 6). At the same time the upper troposphere in southern hemisphere had a high-pressure trend (Figure 4). However after 1984 such notable features as before did not appear. In addition, before 1984 the lower and middle troposphere

over the entire Africa and southern Eurasia seems to have strengthened outflow from the continents to oceans (Figure 5 and 6). Contrastively the upper troposphere over the Africa and southern Eurasia appears to have strengthened inflow from Atlantic and Indian Ocean (Figure 4).

We next show the trend of the velocity potential and the streamfunction at the 0.2101 (upper troposphere) and 0.991 (lower troposphere) sigma levels to diagnose the relation of the divergent and rotation fields in the global scale (Figures 7, 8, 9, 10). Before 1984 the lower troposphere over Africa experienced strengthening trend of the divergence, while the upper troposphere experienced strengthening trend of the convergence (Figure 7 and 8). In contrast, after 1984 the trend shifted in reverse. Additionally the trend shift also occurred over America and the Atlantic Ocean in both hemispheres with reversed phase.

Figures 9 and 10 show the trend of the streamfunction. Before 1984 the lower troposphere above northern Africa experienced strengthening of a cyclonic trend, whereas southern Africa experienced strengthening of an anticyclonic trend. Contrary to the lower troposphere, upper tropospheric trend was in inverse. After 1984 the trend changed to be mostly reversed phase in both lower and upper troposphere.

The trend shift of the specific humidity is shown in Figures 11, 12 and 13. Before 1984 the southern hemisphere experienced wet trends while the areas from northern Africa through Eurasia underwent a dry trend. However after 1984 the wet trend over the southern hemisphere significantly weakened. Sahel experienced the dry trend before 1984, but after 1984 the wet trend occurred from lower through upper troposphere.

Figures 14 and 15 show the trend shift of the thickness between 200hPa and 600hPa, and between 600hPa and 1000hPa. Northern Africa experienced the thinning trend of the thickness from

lower troposphere through upper troposphere before 1984. This trend indicates the cooling over Sahel. In contrast, southern hemisphere experienced the thickening trend, showing warming from lower troposphere through upper troposphere. After 1984 lower troposphere over northern hemisphere, in particular, experienced the thickening trend. These warming and cooling trends are nearly consistent with the trend shift distribution of the global SSTs as described latter sections.

#### **4.3 The vertical structure of the climate shifts**

This subsection describes zonal and meridional vertical atmospheric structures centered at the Sahel region. Figure 16 shows the trends of the meridional circulation averaged between  $20^{\circ}$  W and  $50^{\circ}$  E, in which Africa is located. Before 1984, Sahel experienced a significant large descending trend, whereas the ascending trend over the region around southern Africa. In contrast after 1984 the trend shifted in reverse. Before 1984, Sahel experienced severe dry trend, and contrastively above the southern Atlantic and Indian Ocean experienced marked wet trend (Figure 17). However after 1984 the humidity condition over Sahel shifted, and the lower and middle troposphere experienced a wet trend. Figure 18 shows the trend of the zonal-vertical cross section averaged between equator and  $25^{\circ}$  N. Before 1984 all over northern Africa experienced deep descending trend, and at the same time the Pacific Ocean experienced the same trend while southern America and western Pacific experienced intense ascending trend. After 1984 northwestern Africa experienced ascending trend. Figure 19 additionally show the significant dry trend above Africa before 1984, in contrast the upper troposphere above southern America experienced wet trend. After 1984 the lower troposphere above northwestern Africa and northern tropical Atlantic show the wet trend.

#### 4.4 Global SST trends

Here we describe the shift of the global SST trend. Upper and lower panels of Figure 20 respectively show the SST trend before and after 1984. North-south interhemispheric anti-symmetric pattern is obvious in both panels with reversed phases. The SST in the northern hemisphere overall experienced cooling trend before 1984, whereas warming trend in the southern hemisphere. After 1984, in contrast, warming trend occurred in the northern hemisphere, whereas cooling trend around the Antarctica can be seen. This interhemispheric SST pattern suggests that the north-south inter-hemispheric contrast of the SST influenced the precipitation variability in Sahel. We also show the area-averaged SST trends between 20° W through 50° E (Figure 21). The contrast of the trend shift in northern hemisphere compared with southern hemisphere is also obvious. Before 1984, the SST indicates the warming trend in the southern hemisphere as compared with the northern hemisphere, in contrast after 1984, the pattern was overall in reverse. The area-averaged SST trends between 0° N through 25° N are shown in Figure 22. The SST for this zonal cross section indicates that the SST trend except for eastern Pacific shifted much larger after 1984 than before 1984.

Based on these results, here we define a North-South SST polarity index (NS-SST index) that is the subtraction of the SST averaged all over the southern hemisphere (black line in Figure 23) from the SST averaged all over the northern hemisphere (orange line in Figure 23). Figure 24 shows time series of both the NS-SST index and the precipitation in the Sahel region. The time series of the NS-SST index signifies the minimal value in 1984 and the trend of the NS-SST index showed decreasing trend before 1984 and after 1984 an increasing trend is obvious. This feature is remarkably similar to the precipitation variability in Sahel. Lag-correlation between the NS-SST

index and the precipitation in Sahel is listed in Table 1. Obviously, the NS-SST index precedes the Sahel precipitation, and the maximum correlation is in 2-year difference.

To demonstrate the importance of the north-south inter-hemispheric contrast of the entire ocean, not of the individual ocean, we calculate the lag-correlation between the precipitation variability in Sahel and the NS-SST index, and the other SST index which is obtained by subtracting the SST averaged over the southern Atlantic from that averaged over northern Atlantic (NS Atlantic SST index), for Indian ocean (NS Indian SST index), and for Pacific ocean (NS Pacific SST index) (Figure 25). The correlation coefficient of the NS-SST index exceeds those of the other SST indices, suggesting that the precipitation variability in Sahel strongly associated with the north-south interhemispheric contrast of the entire ocean rather than that of the individual ocean.

#### **4.5 North-South SST polarity index and its associated patterns**

In this subsection we show the relationship of the NS-SST index with the global SST and land precipitation. Figure 26 shows the negative correlation over the southern hemispheric ocean centered around Atlantic and Indian ocean, in contrast, the positive correlation is overall seen in the northern hemisphere. This north-south interhemispheric SST contrast is highly consistent with the global SST trend shift. In addition, we examine the correlation between the NS-SST index and the global precipitation (Figure 27). The positive correlation appears over Sahel and northern Eurasia, contrastingly the negative correlation appears around southern America and central Australia. These situations are also similar to the trend shift of the global precipitation (Figure 3). According to the time series of the NS-SST index (Figure 24), the recent features of the global SST are linked to the warm SSTs over the northern hemisphere relative to those of the southern hemisphere, and trends

over Sahel and northern Eurasia show the increase of the annual precipitation while the annual precipitation over South America and central Australia declined.

Next we show the correlation between the NS-SST index and the other atmospheric fields as shown in previous figures. Figure 28 shows that the upper troposphere above northern Africa shows the positive correlation, and in contrast, the regions above the Atlantic and South America have negative correlation. At the same time, the lower troposphere around entire Africa has negative correlation coefficients, whereas southern America and around South Pole have positive correlation. In addition, negative correlation can be seen at the upper troposphere above northern Africa and tropical Atlantic, while the areas above South America and the tropical Atlantic have positive correlation (Figure 29). Contrary to the upper troposphere, the correlations in the lower troposphere correlation are in inverse.

We also demonstrate the correlation between the NS-SST index and the global specific humidity (Figure 30). From the lower troposphere through upper troposphere over the northern hemisphere positive correlation can be seen, whereas in the southern hemisphere negative correlation is seen. We further exhibit the vertical cross section of the correlation of the NS-SST index with the specific humidity, and meridional and zonal circulations (Figures 31, 32, 33 and 34). Both circulations show the ascending and wet over Sahel, and in contrast southern Africa and America show the descending and dry conditions. In particular, the meridional cross section of the specific humidity signifies notable contrast; Sahel experienced wet, while the South Atlantic and Indian Ocean is dry.

## 5. Discussion and Conclusion

We have confirmed that Sahel experienced rapid decreasing trend of the annual mean precipitation before 1984. In contrast, after 1984, it experienced increasing trend. This trend shift is in agreement with previous studies [Hagos and Cook 2008, Hoerling et al. 2006, Fall et al. 2006]. We have found that the shifts of the precipitation trend occurred not only within Sahel but also over the many regions on the earth. In particular the trend shift in the pan-Eurasian area along with Africa is overall in phase, whereas the shift in the Pan-American area along with Australia is overall out-of-phase to the pan-Eurasia.

The precipitation variability in Sahel in the interannual time scale is remarkably similar to that of the North-South SST polarity that is the SST contrast between the area-averaged SSTs in the Southern Hemisphere and in the Northern Hemisphere. When the SST in the Southern Hemisphere was colder than that of the Northern Hemisphere, the precipitation in Sahel was larger than normal. Our North-South SST polarity index successfully captured the recent increasing trend of the precipitation in Sahel whereas decrease trend before 1984, so that we could confirm the previous study in Folland et al. [1986], in which the North-South SST polarity accounted for the decreasing trend occurring in 1960-70, but did not examine recovery after 1980s. The North-South SST polarity index, which includes entire oceans on the earth, accounted for the precipitation variability in Sahel more than that of North-South SST polarity index of an individual ocean. In addition, our North-South SST polarity index successfully accounts for the trend shift over other regions, e.g., Eurasia, Australia and South America.

The trend of the SST contrast is also in association with the trends of global-scale meridional and zonal atmospheric circulations. In years in increasing trend in Sahel precipitation, strengthening

trend of updraft over Sahel along with increase of specific humidity in both meridional and zonal circulations. These results suggest that the North-South SST contrast determines the precipitation trends on the earth through the change of global atmospheric circulations. Further studies on the causes of long-term variation of the SST polarity between the Northern and Southern Hemispheres must be examined in future.

## **Acknowledgements**

I really express my appreciation to the individuals and many groups of people who have helped me directly and indirectly over years with various aspects of writing this thesis. First, I am deeply grateful to my academic advisor Prof. Yoshihiro Tachibana who taught me generously and gave so many valuable ideas, suggestions and comments concerned with the global climate variability and studying methods. I am especially grateful to Prof. Kaoru Fukuyama and Prof. Yoshihiko Sekine and the other Professors for their lectures, seminars and valuable suggestions and comments to my research. I faithfully express my appreciation to the GPCC for the precipitation data; the NOAA-CIRES Climate Diagnostics Center, Boulder, Colorado, USA for the atmospheric field datum; NOAA/OAR/ESRL PSD, Boulder, Colorado, USA for the global SST data. I would like to appreciate the gratitude to Mr. Yuji Higashi for his kind teaching and technical supports to me in the applications of computer hardware and software for my study and research works. Finally I am also thankful to my good classmates, friends and colleagues in Geosystem Science for their kind helps and warmth in my campus life in Mie University.

## References

- Fall, S.; M. H. F. Semazzi; D. D. S. Niyogi; R. O. Anyah; J. Bowden. The spatiotemporal climate variability over Senegal and its relationship to global climate. *International Journal of Climatology*. 2006, No.26, p.2057-2076.
- Folland, C. K.; T. N. Palmer; D. E. Parker. Sahel rainfall and worldwide sea temperatures, 1901-85. *Nature*. 1986, Vol.302, p.602-607, doi:10.1038/320602a0.
- Folts, G. R. and M. J. McPhaden. Trends in Saharan dust and tropical Atlantic climate during 1980-2006. *Geophysical Research Letters*. 2008, Vol.35, L20706, doi:10.1029/2008GL035042.
- Giannini, A.; R. Sravanan; P. Chang. Oceanic Forcing of Sahel Rainfall on Interdecadal Time Scales. *Science*, 2003, Vol.302, p.1027-1030.
- Griffiths, J.F. "The Northern Desert (Sahara)". *Climates of Africa*. New York, Elsevier, 1972, p.75-131.
- Hagos, S. M. and K. H. Cook. Ocean Warming and Late-Twentieth-Century Sahel Drought and Recovery. *Journal of Climate*. 2008, Vol.21, No.15, pp.3797-3814.
- Heumann, B. W.; J. W. Seaquist; L. Eklundh; P. Jonsson. AVHRR derived phenological change in the Sahel and Soudan, Africa, 1982-2005. *Remote Sensing of Environment*. 2007, Vol.108, p.385-392.

- Hoerling, M.; J. Hurrell; J. Eischeid; A. Phillips. Detection and Attribution of Twentieth-Century Northern and Southern African Rainfall Change. *Journal of Climate*. 2006, Vol.19, p.3989-4008.
- Hountondji, Y. C.; N. Sokpon; P. Ozer. Analysis of the vegetation trends using low resolution remote sensing data in Burkina Faso (1982-1999) for the monitoring of desertification. *International Journal of Remote Sensing*. 2006, Vol.27, No.5, p.871-884.
- Kalnay, E.; M. Kanamitsu; R. Kistler; W. Collins; D. Deaven; L. Gandin; M. Iredell; S. Saha; G. White; J. Woollen; Y. Zhu; A. Leetmaa, R. Reynolds; M. Chellian; W. Ebisuzaki; W. Higgins; J. Janowiak; K. C. Mo; R. Jenne; D. Joseph. The NCEP/NCAR 40-year Reanalysis Project. *Bulletin of the American Meteorological Society*. 1996, Vol.77, p.437-471.
- Nicholson, E. S. and P. J. Webster. A physical basis for the interannual variability of rainfall in the Sahel. *Quarterly of the Royal Meteorological Society*. 2007, doi:10.1002/qj.104.
- Nieto, R.; L. Gimeno; R. M. Trigo. A Lagrangian identification of major sources of Sahel moisture. *Geophysical Research Letters*. 2006, Vol.33.
- Omotosho, B. J.. Pre-rainy season moisture build-up and storm precipitation delivery in the West African Sahel. *International Journal of Climatology*. 2008, Vol.28, p.937-946, doi:10.1002/joc.1548.

Schneider, U.; T. Fuchs; A. M. Christoffer; B. Rundolf. Global Precipitation Analysis Product of the GPCC. Deutscher Wetterdienst, Offenbach a. M., Germany, Nov. 2008, p.1-12.

Smith, T. M.; R. W. Reynolds; T. C. Peterson; J. Lawrimore. Improvements to NOAA's Historical Merged Land-Ocean Surface Temperature Analysis (1880-2006). *Journal of Climate*. In press.

Thiaw, W. M. and K. C. Mo. Impact of Sea Surface Temperature and Soil Moisture on Seasonal Rainfall Prediction over the Sahel. *Journal of Climate*. 2005, Vol.18, p.5330-5343.

Xue, Y.; T. M. Smith; R. W. Reynolds. Interdecadal changes of 30-yr SST normals during 1871-2000. *Journal of Climate*. 2003, Vol.16, p.1601-1612.

## Figure caption

Fig.1 Climatological annual precipitation (mm/year) in northwestern Africa and the Sahel region (100 ~ 500 mm/year). Black lines indicate isohyetal lines at the 100 and 500 mm/year.

Fig.2 Normalized yearly precipitation anomalies and their linear regression lines before 1984 and after 1984.

Fig.3 Trends of normalized precipitation anomalies before 1984 (top) and after 1984 (bottom). Bluish (Brownish) color indicates increasing (decreasing) trends and contour intervals are 0.03. Shaded areas are significant at the 1%, 5%, 10% levels based on a Student's t-test.

Fig.4 Trends of normalized geopotential heights (contour) and horizontal winds (vector) at 200hPa before 1984 (top) and after 1984 (bottom). Reddish (Bluish) color indicates high-pressure (low-pressure) trends and contour intervals are 0.03. Shaded areas are the same as Fig.3.

Fig.5 As in Fig.4 except for at 600hPa.

Fig.6 As in Fig.4 except for at 1000hPa.

Fig.7 Trends of normalized velocity potential at 0.2101 sigma level before 1984 (top) and after

1984 (bottom). Reddish (Bluish) color indicates divergent (convergent) trends and contour intervals are 0.03. Shaded areas are the same as Fig.3.

Fig.8 As in Fig.7 except for at 0.995 sigma level.

Fig.9 Trends of normalized streamfunction at 0.2101 sigma level before 1984 (top) and after 1984 (bottom). Reddish (Bluish) color indicates counterclockwise (clockwise) trends and contour intervals are 0.03. Shaded areas are the same as Fig.3.

Fig.10 As in Fig.9 except for at 0.995 sigma level.

Fig.11 Trends of the specific humidity at 300hPa before 1984 (top) and after 1984 (bottom). Bluish (Brownish) color indicates wet (dry) trends and contour intervals are 0.03. Shaded areas are the same as Fig.3.

Fig.12 As in Fig.11 except for at 600hPa.

Fig.13 As in Fig.11 except for at 1000hPa.

Fig.14 Trends of normalized thickness between 200hPa and 600hPa before 1959 (top) and after

1984 (bottom). Reddish (Bluish) color indicates thick (thin) trends and contour intervals are 0.03.

Shaded areas are the same as Fig.3.

Fig.15 As in Fig.14 except for between 600hPa and 1000hPa.

Fig.16 Vertical cross section of the trends of the meridional and vertical winds averaged from 20° W through 50° E before 1984 (top) and after 1984 (bottom). Reddish (Bluish) color indicates northward and upward (southward and downward) trends and contour intervals are 0.03. Shaded areas are the same as Fig.3.

Fig.17 Vertical cross section of the trends of the specific humidity averaged from 20° W through 50° E before 1984 (top) and after 1984 (bottom). Bluish (Brownish) color indicates wet (dry) trends and contour intervals are 0.03. Shaded areas are the same as Fig.3.

Fig.18 As in Fig.16 except for the trend of the zonal and vertical winds averaged from equator through 25° N and that reddish (bluish) color indicates eastward and upward (westward and downward) trends.

Fig.19 As in Fig.17 except for the trends of the specific humidity averaged from equator through 25° N.

Fig.20 Trends of SST between before 1984 (top) and after 1984 (bottom). Reddish (Bluish) color indicates warming (cooling) trend and contour intervals are 0.03. Shaded areas are the same as Fig.3.

Fig.21 SST trends averaged from 20° W through 50° E. Vertical axis is SST trend and horizontal axis is latitude. Dark blue (Orange) lines depict the trends before (after) 1984.

Fig.22 SST trends averaged from equator through 25° N. Vertical axis is SST trend and horizontal axis is longitude. Dark blue (Orange) lines depict the trends before (after) 1984.

Fig.23 Time series of normalized SST anomalies averaged within northern (orange) and southern (black) hemisphere.

Fig.24 Normalized precipitation anomalies (orange) in Sahel and North-South SST polarity index that is the subtraction of the SST averaged all over the southern hemisphere from the SST averaged all over the northern hemisphere (dark blue), and their linear regression lines before 1984 and after 1984.

Fig.25 Lag-correlation between Sahel precipitation anomaly and NS-SST polarity index (dark blue), North-South Atlantic SST polarity index (Orange), North-South Indian SST polarity index (black), and North-South Pacific SST polarity index (green).

Fig.26 Correlations between the NS-SST index and the global SST for the time lag of 0 year. Reddish (Bluish) color indicates positive (negative) correlations and contour intervals are 0.2. Shaded areas are the same as Fig.3.

Fig.27 Correlations between the NS-SST index and the normalized precipitation anomalies for the time lag of 0 year. Bluish (Brownish) color indicates positive (negative) correlations and contour intervals are 0.2. Shaded areas are the same as Fig.3.

Fig.28 As in Fig.26 except for between the NS-SST index and velocity potential at 0.2101 sigma level (top) and at 0.995 sigma level (bottom).

Fig.29 As in Fig.28 except for between the NS-SST index and streamfunction.

Fig.30 As in Fig.27 except for between the NS-SST index and the specific humidity at 300hPa (top), 600hPa (middle), 1000hPa (bottom) and that bluish (brownish) color indicates positive (negative) correlations.

Fig.31 Vertical cross section of the correlations between NS-SST index and the meridional and vertical winds averaged from 20° W through 50° E. Reddish (Bluish) color indicates positive (negative) correlations and contour intervals are 0.03. Shaded areas are the same as Fig.3.

Fig.32 Vertical cross section of the correlations between NS-SST index and the specific humidity averaged from 20° W through 50° E. Bluish (Brownish) color indicates positive (negative) correlations and contour intervals are 0.03. Shaded areas are the same as Fig.3.

Fig.33 As in Fig.31 except for the zonal and vertical winds averaged from equator through 25° N.

Fig.34 As in Fig.32 except for the specific humidity averaged from equator through 25° N.

Fig.1A Ratio of monthly precipitation with the annual precipitation averaged from 1959 through 2007.

Fig.2A Trends of the atmospheric stability between 200hPa and 600hPa before 1984 (top) and after 1984 (bottom). Reddish (Bluish) color indicates stable (unstable) trends and contour intervals are 0.03. Shaded areas are the same as Fig.3.

Fig.3A As in Fig.2A except for between 600hPa and 1000hPa.

**Table caption**

Table 1 Lag-correlations between the North-South SST polarity index and Sahel precipitation

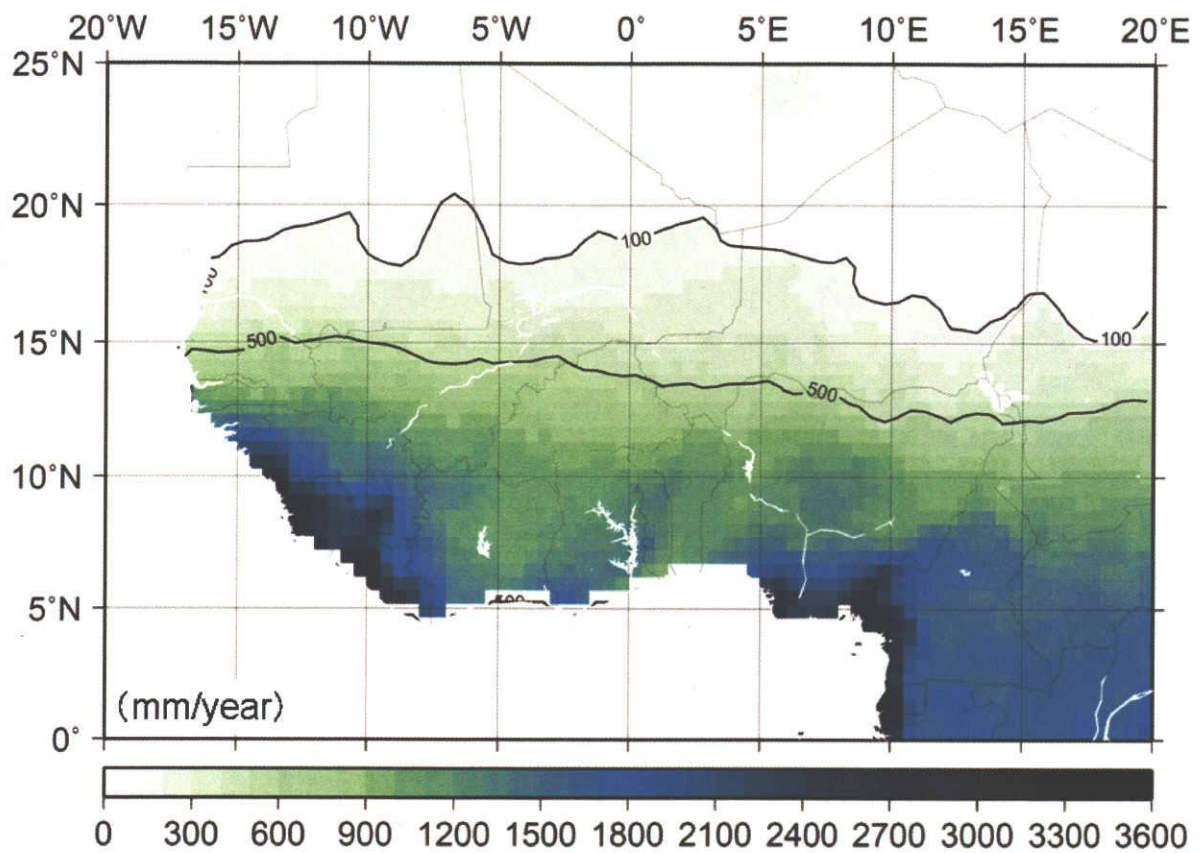


Fig.1 Climatological annual precipitation (mm/year) in northwestern Africa and the Sahel region (100 ~ 500 mm/year). Black lines indicate isohyetal lines at the 100 and 500 mm/year.

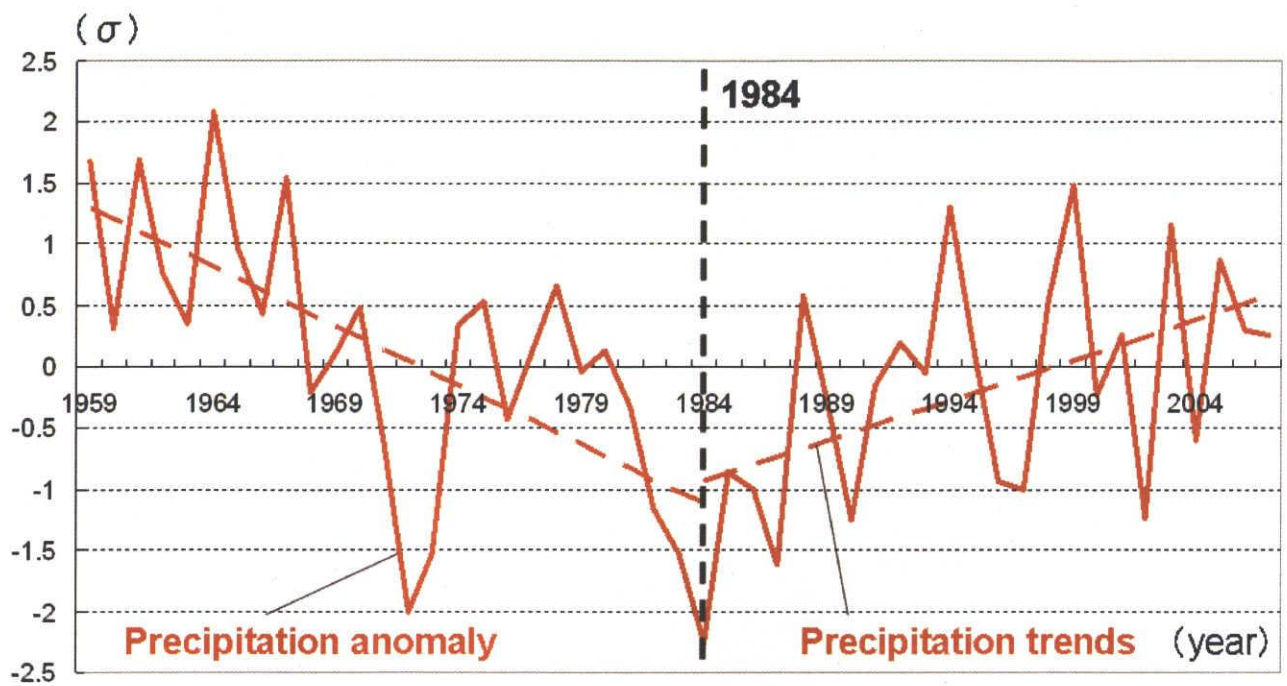


Fig.2 Normalized yearly precipitation anomalies and their linear regression lines before 1984 and after 1984.

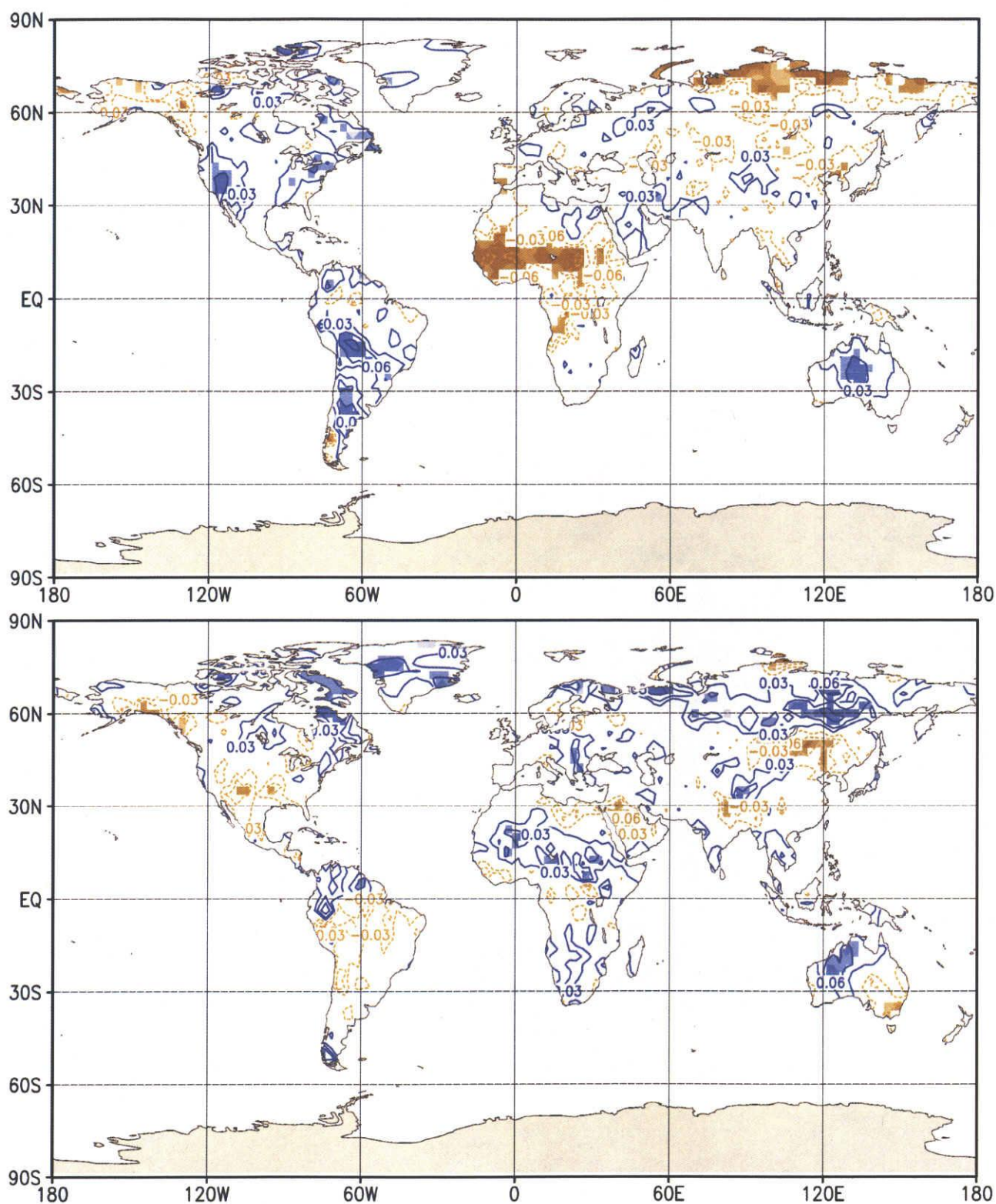


Fig.3 Trends of normalized precipitation anomalies before 1984 (top) and after 1984 (bottom). Bluish (Brownish) color indicates increasing (decreasing) trends and contour intervals are 0.03. Shaded areas are significant at the 1%, 5%, 10% levels based on a Student's t-test.

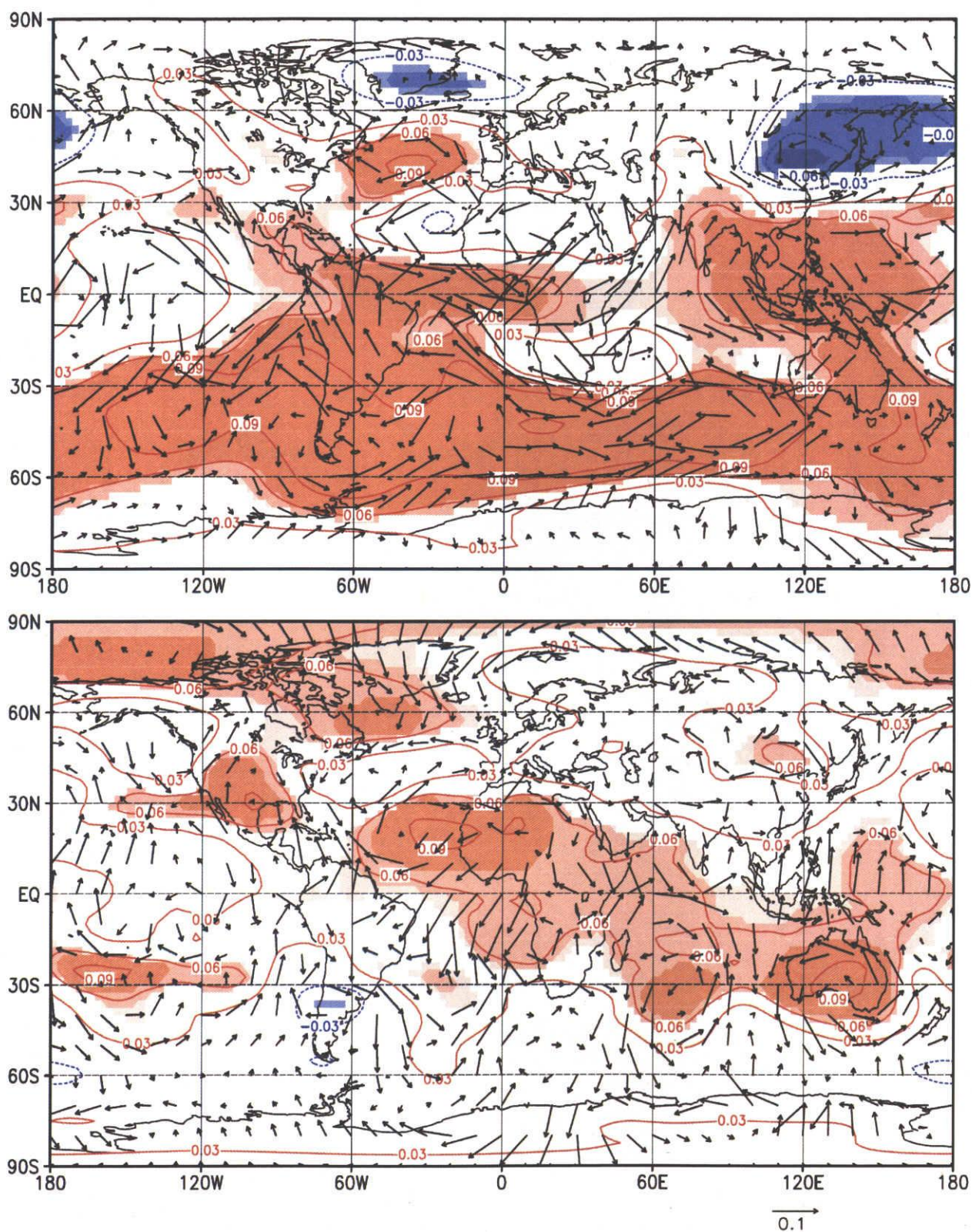


Fig.4 Trends of normalized geopotential heights (contour) and horizontal winds (vector) at 200hPa before 1984 (top) and after 1984 (bottom). Reddish (Bluish) color indicates high-pressure (low-pressure) trends and contour intervals are 0.03. Shaded areas are the same as Fig.3.

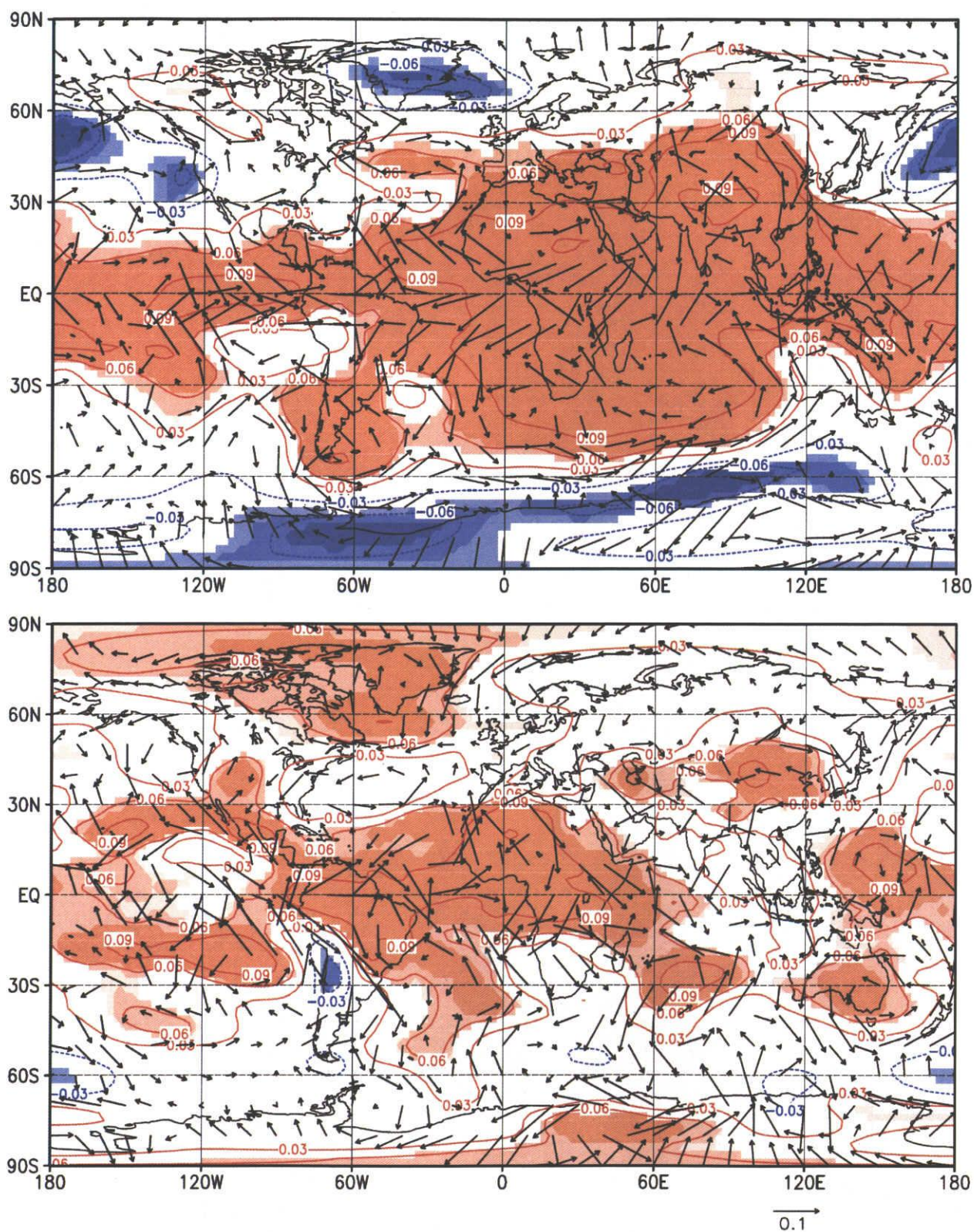


Fig.5 As in Fig.4 except for at 600hPa.

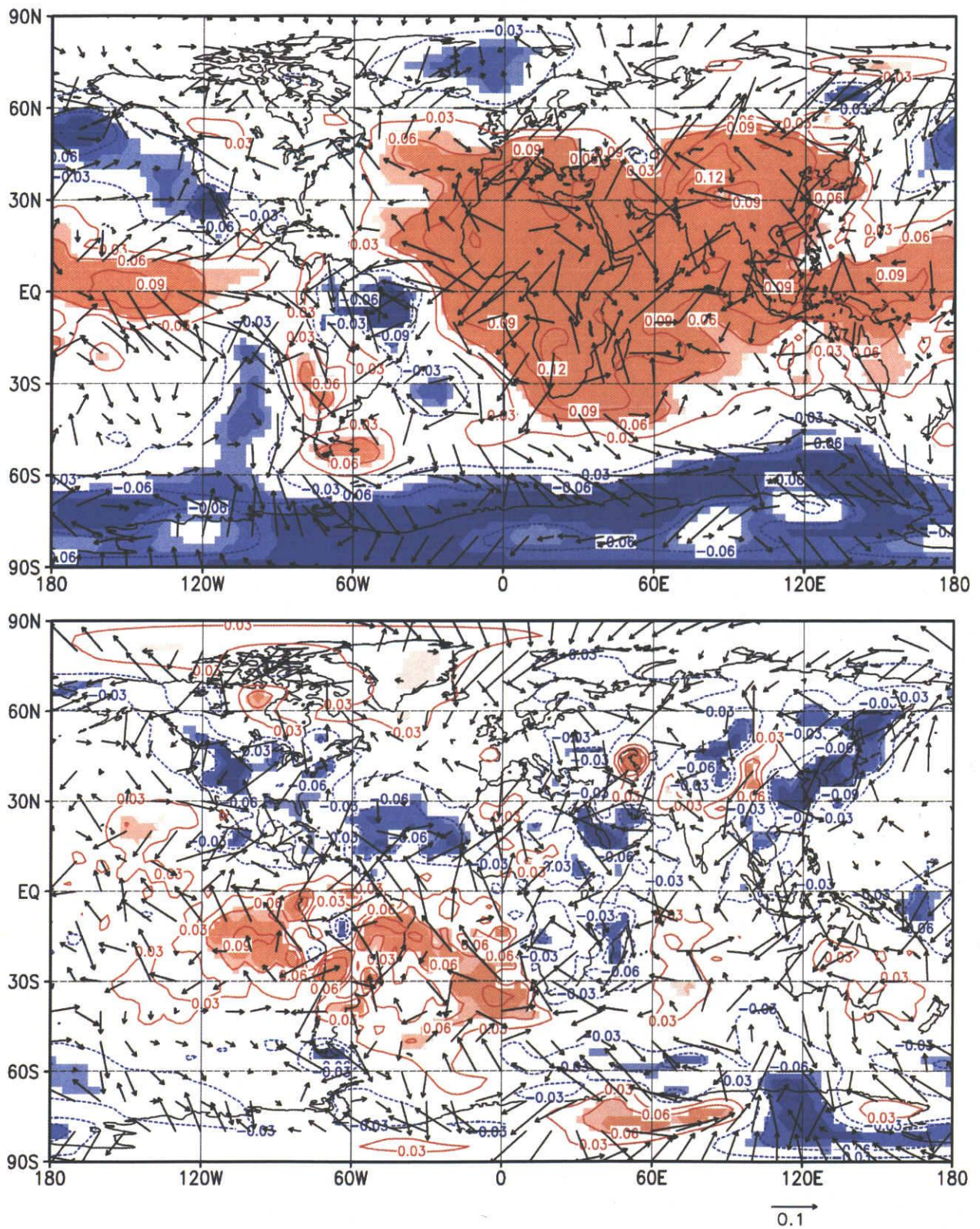


Fig.6 As in Fig.4 except for at 1000hPa.

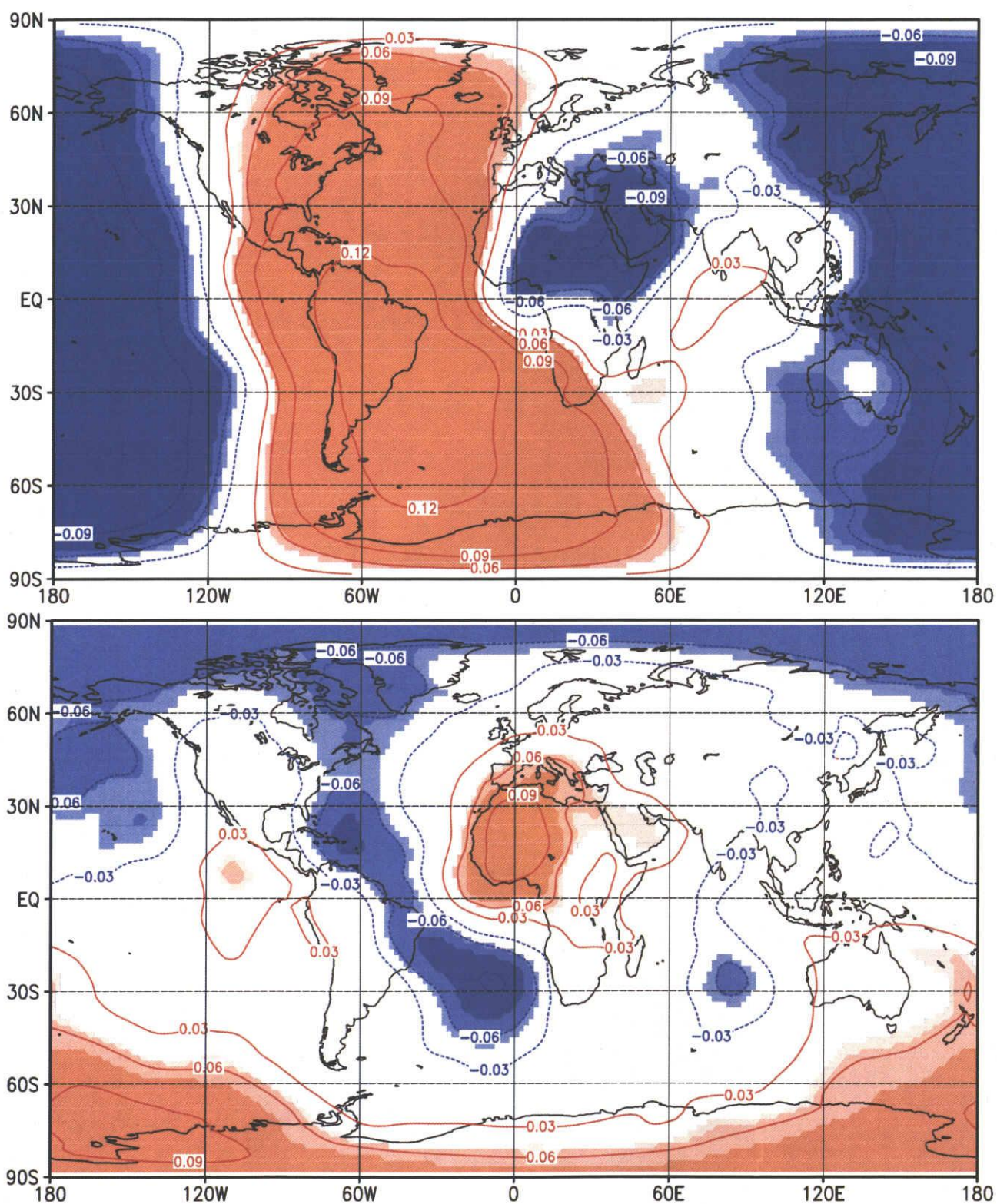


Fig.7 Trends of normalized velocity potential at 0.2101 sigma level before 1984 (top) and after 1984 (bottom). Reddish (Bluish) color indicates divergent (convergent) trends and contour intervals are 0.03. Shaded areas are the same as Fig.3.

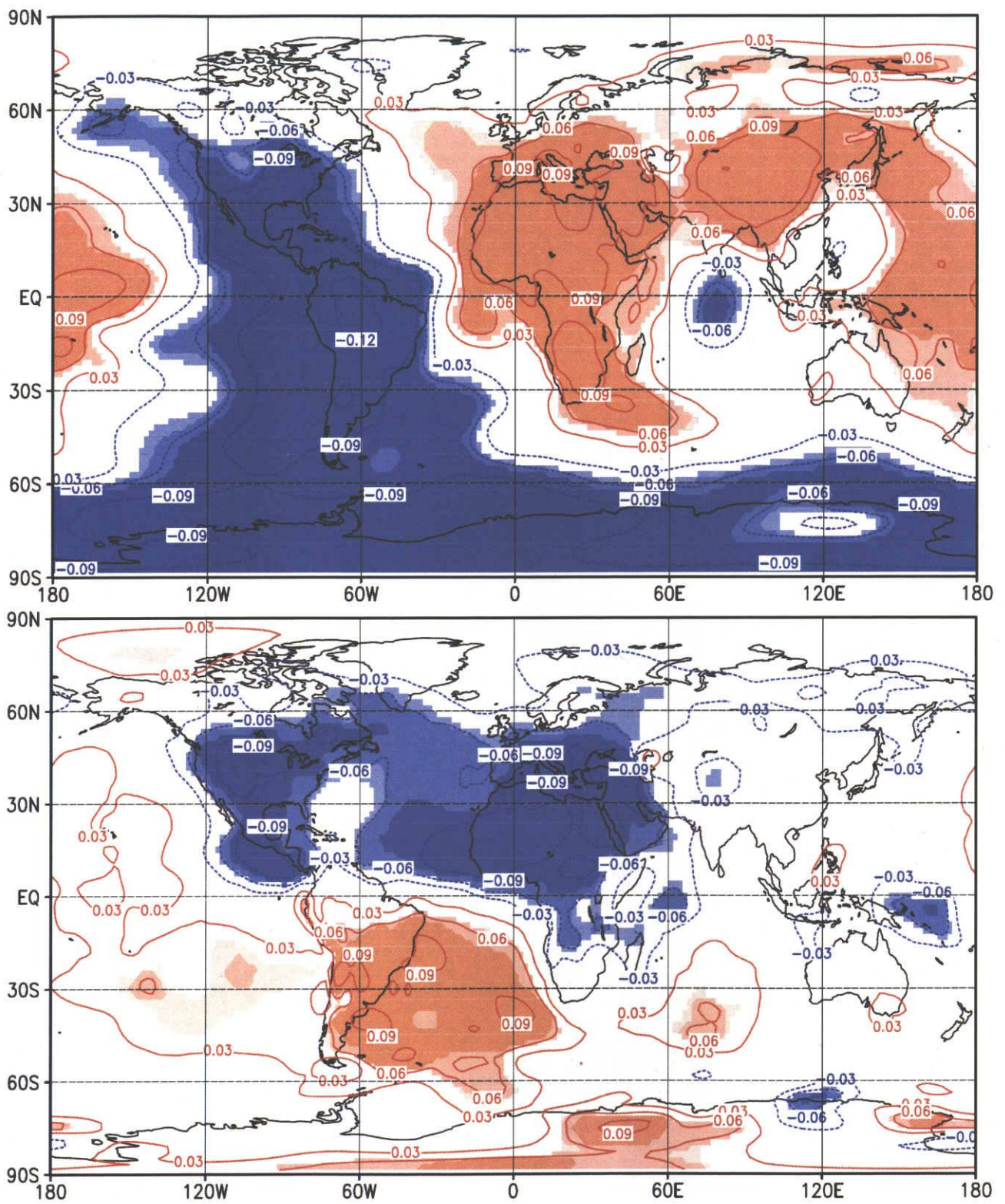


Fig.8 As in Fig.7 except for at 0.995 sigma level.

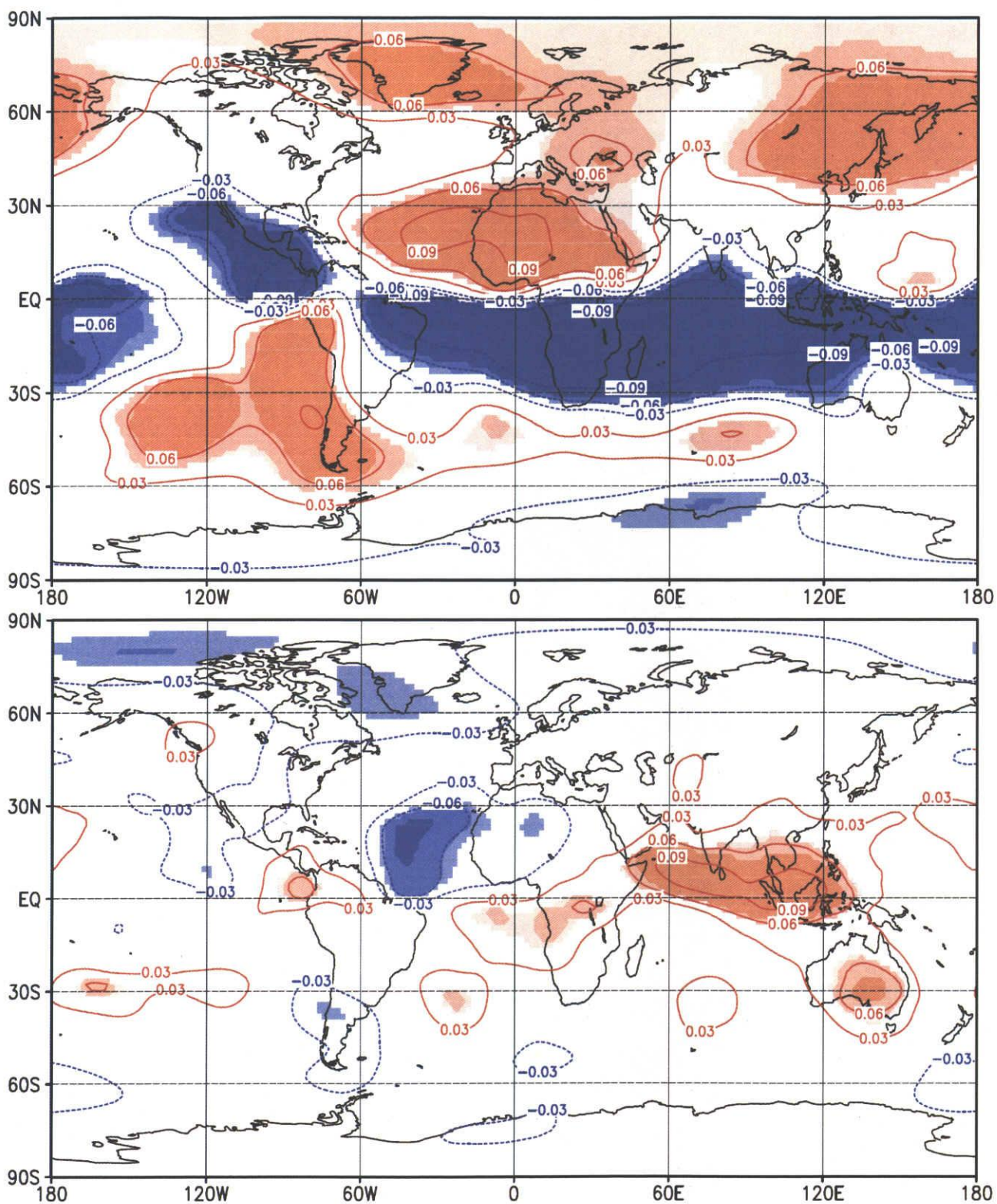


Fig.9 Trends of normalized streamfunction at 0.2101 sigma level before 1984 (top) and after 1984 (bottom). Reddish (Bluish) color indicates counterclockwise (clockwise) trends and contour intervals are 0.03. Shaded areas are the same as Fig.3.

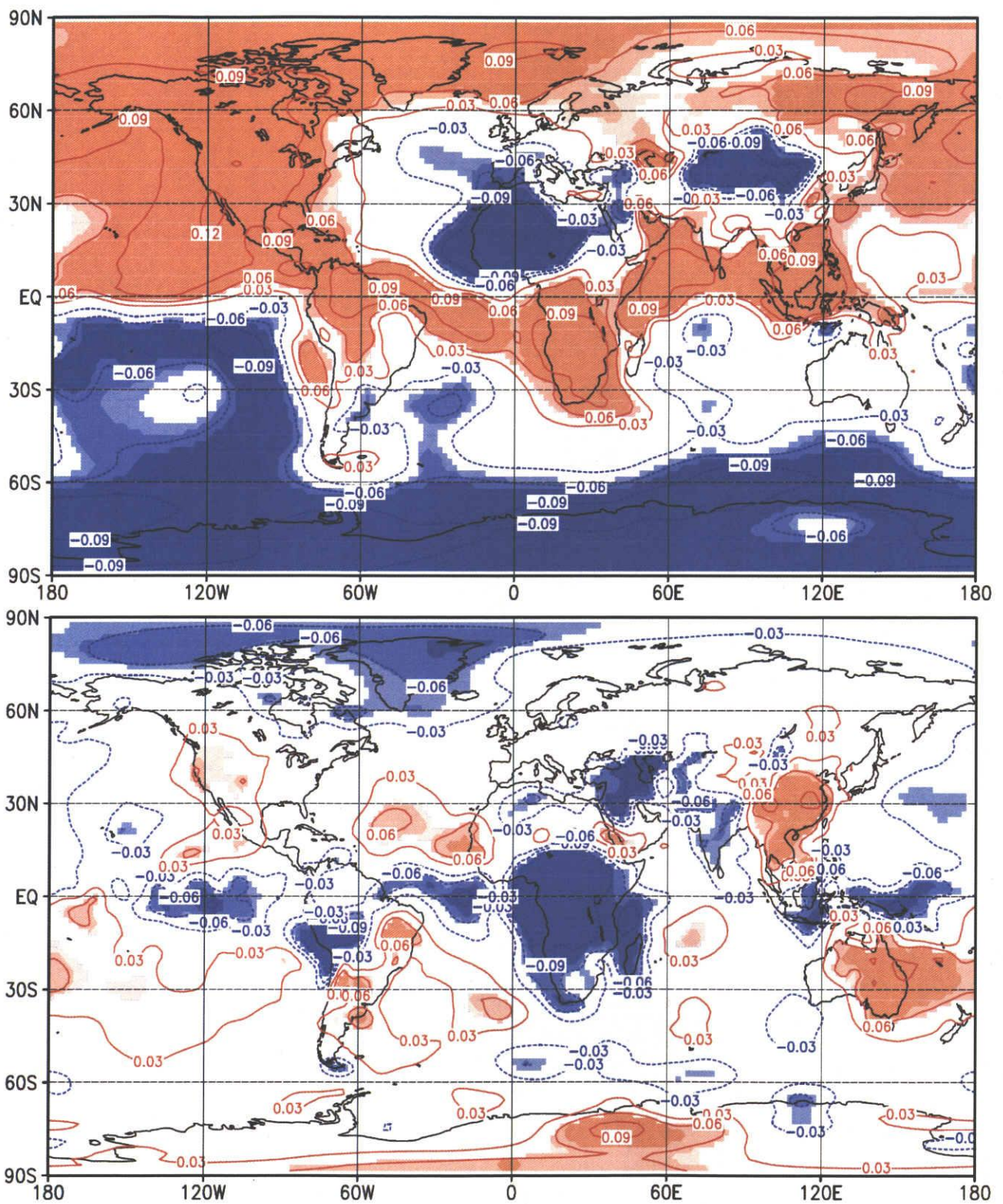


Fig.10 As in Fig.9 except for at 0.995 sigma level.

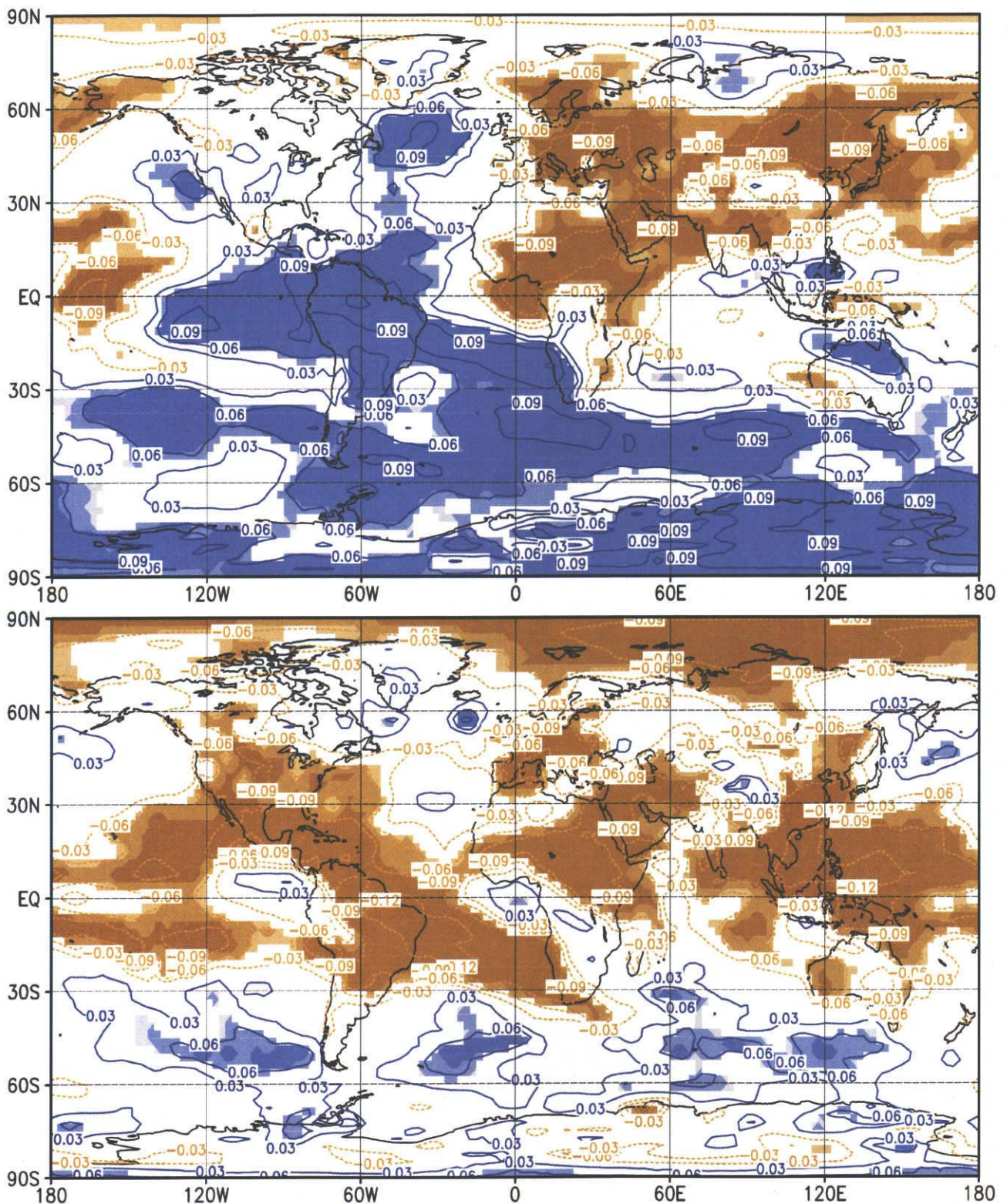


Fig.11 Trends of the specific humidity at 300hPa before 1984 (top) and after 1984 (bottom). Bluish (Brownish) color indicates wet (dry) trends and contour intervals are 0.03. Shaded areas are the same as Fig.3.

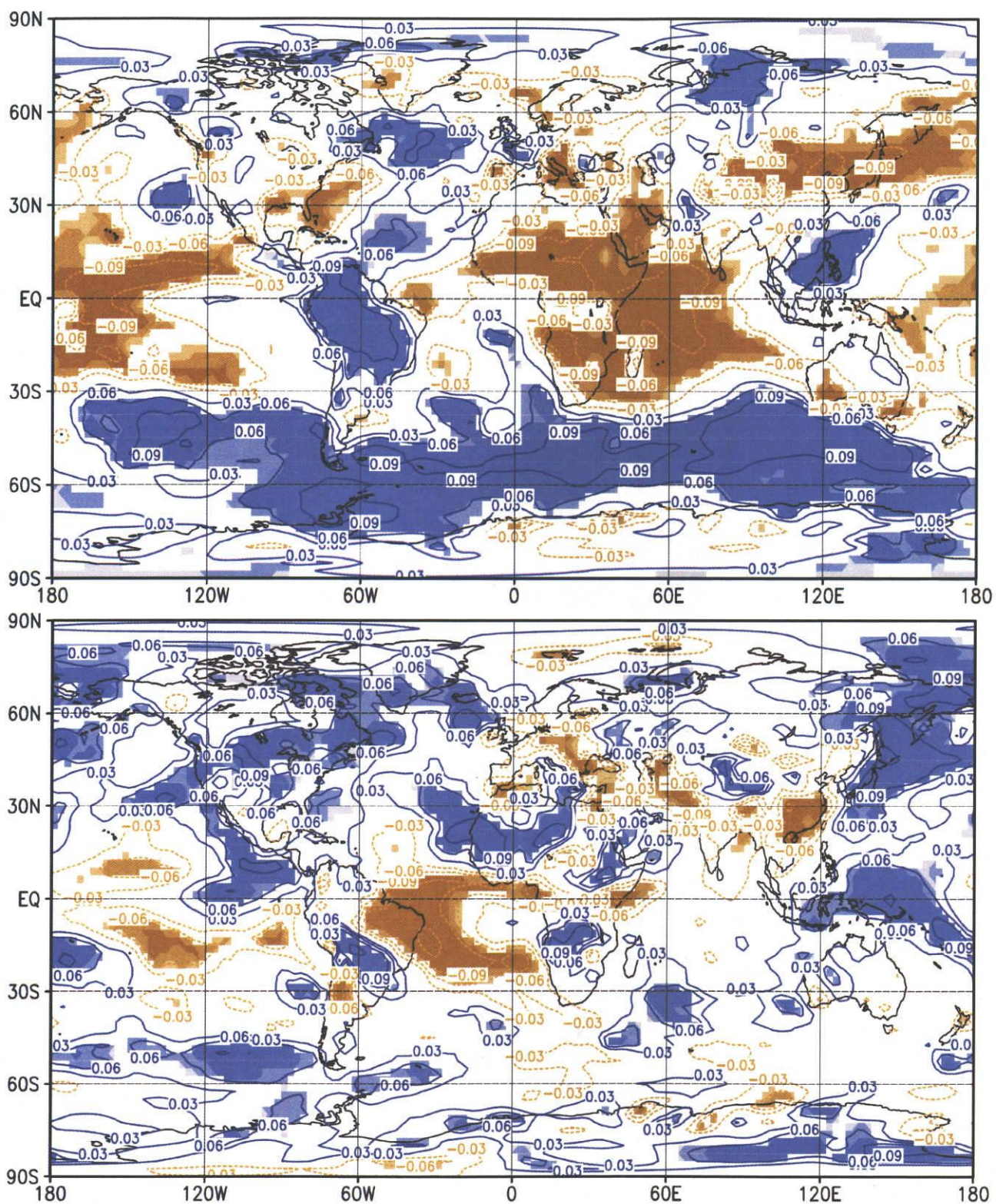


Fig.12 As in Fig.11 except for at 600hPa.

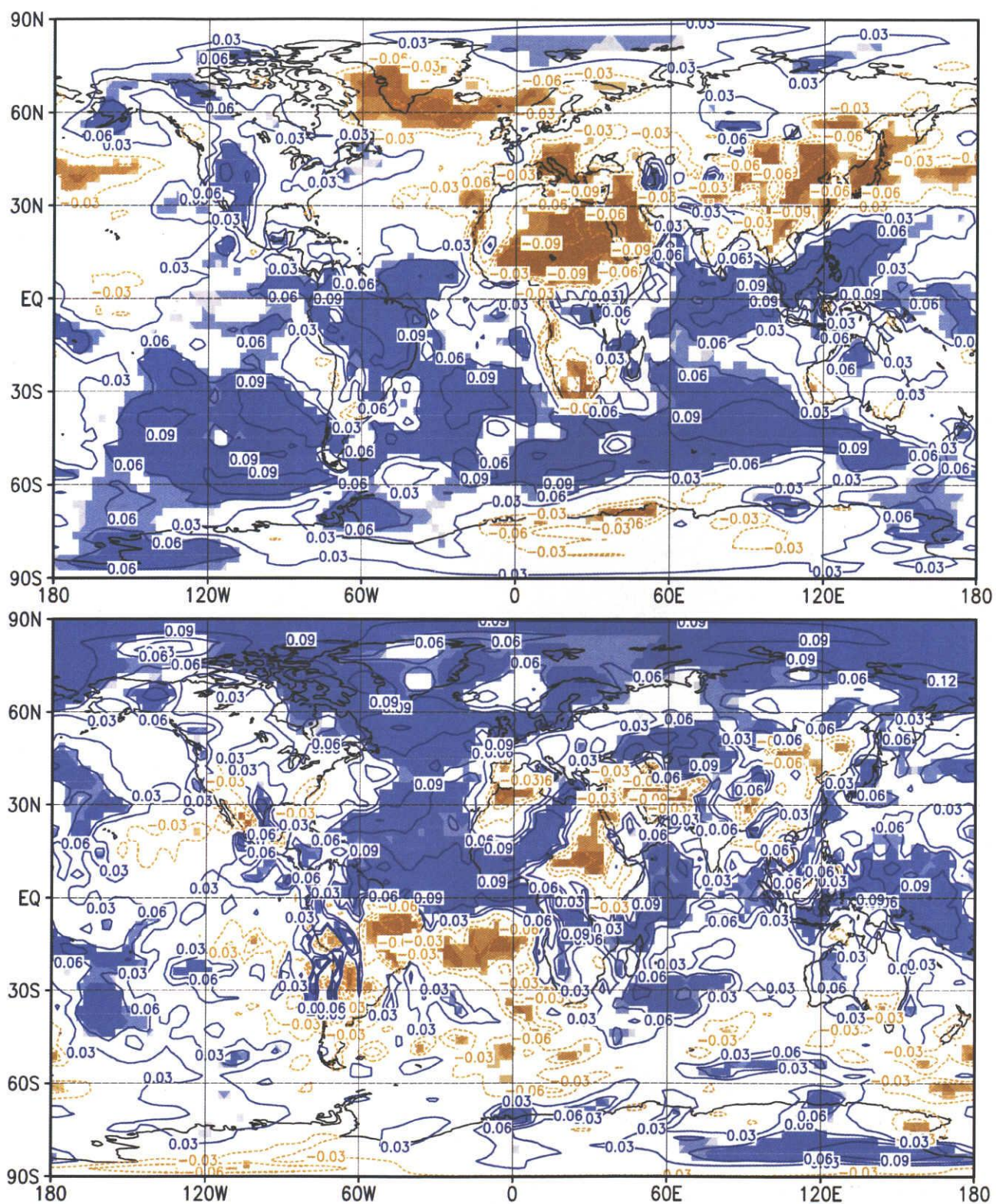


Fig.13 As in Fig.11 except for at 1000hPa.

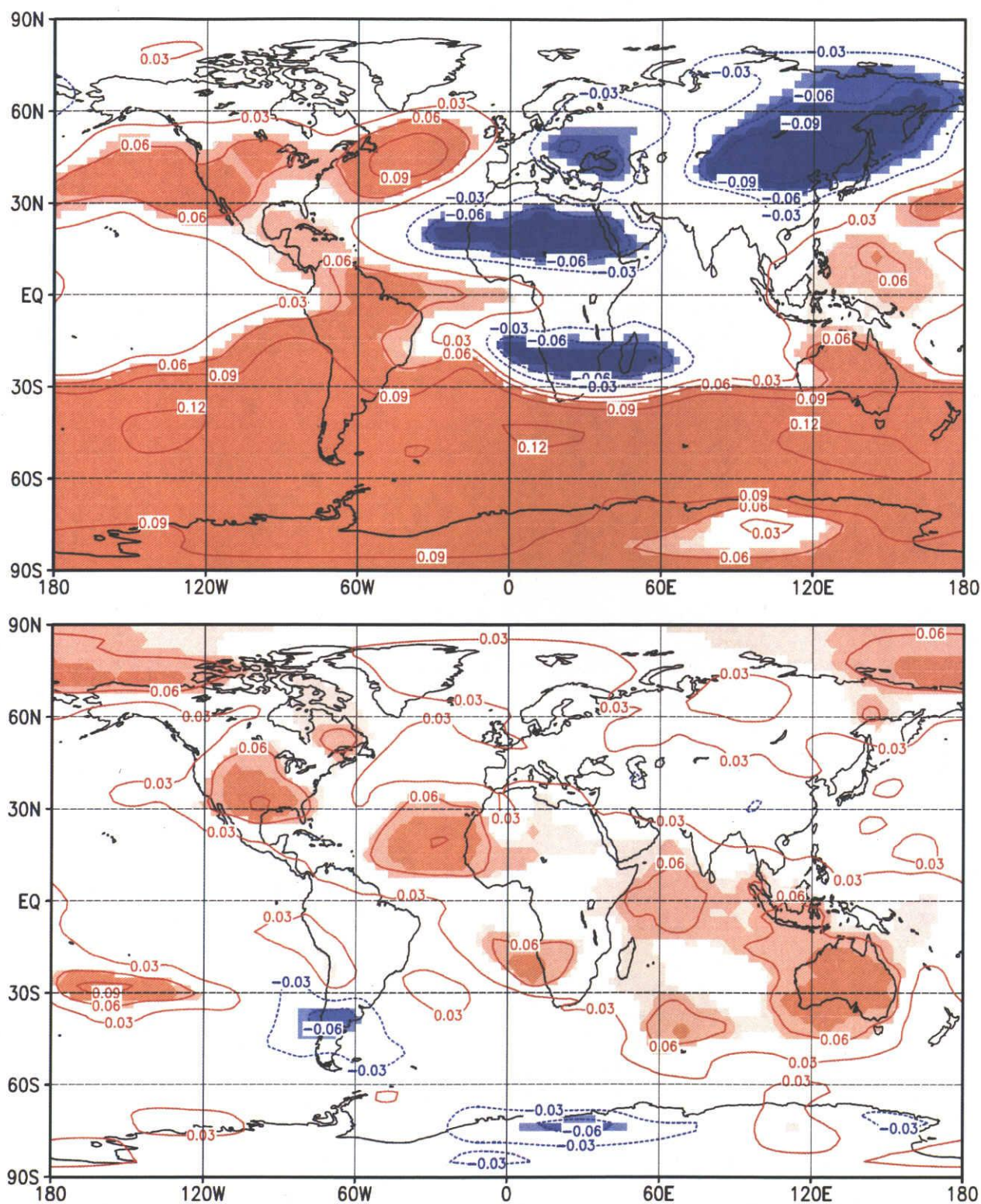


Fig.14 Trends of normalized thickness between 200hPa and 600hPa before 1959 (top) and after 1984 (bottom). Reddish (Bluish) color indicates thick (thin) trends and contour intervals are 0.03. Shaded areas are the same as Fig.3.

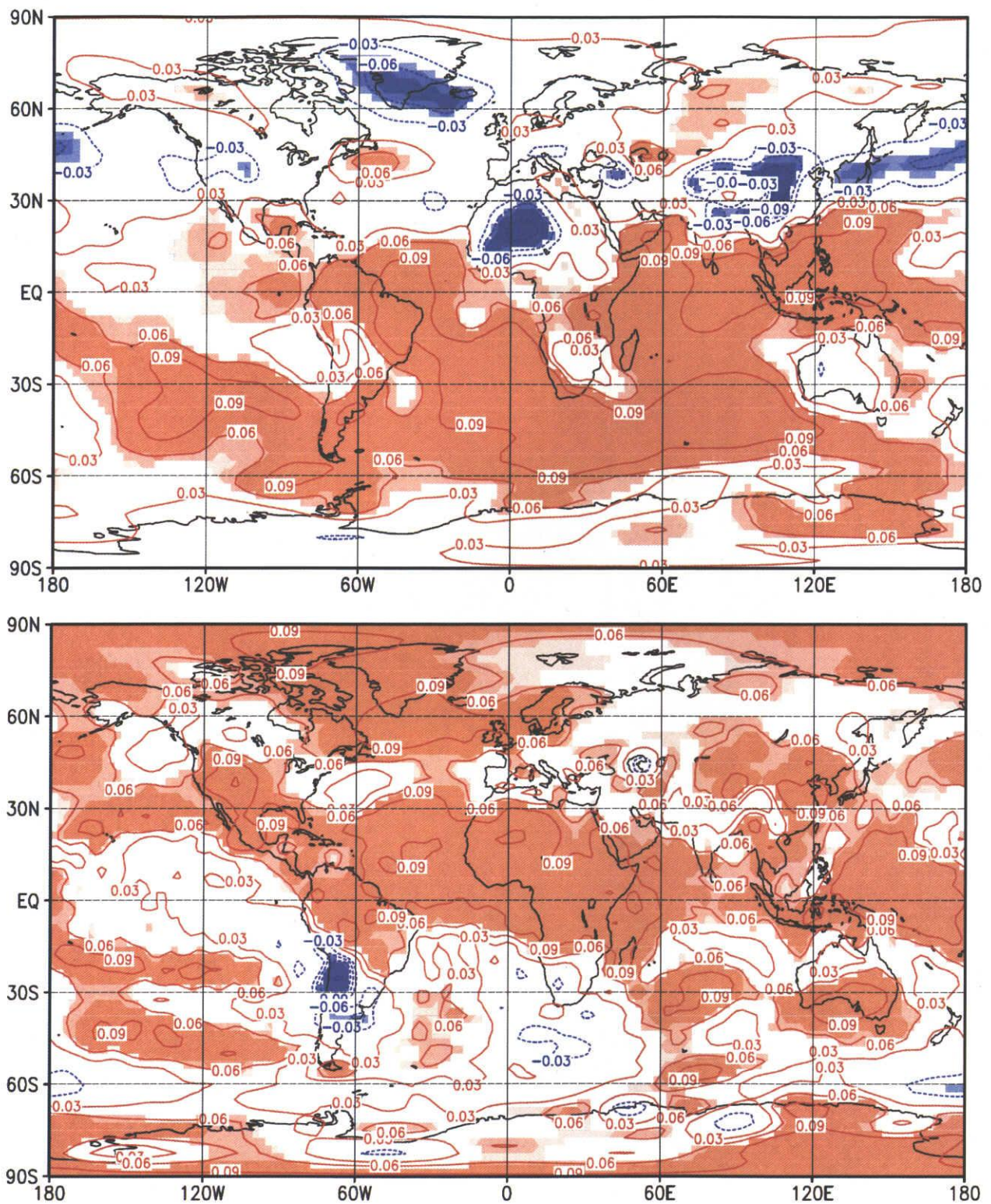


Fig.15 As in Fig.14 except for between 600hPa and 1000hPa.

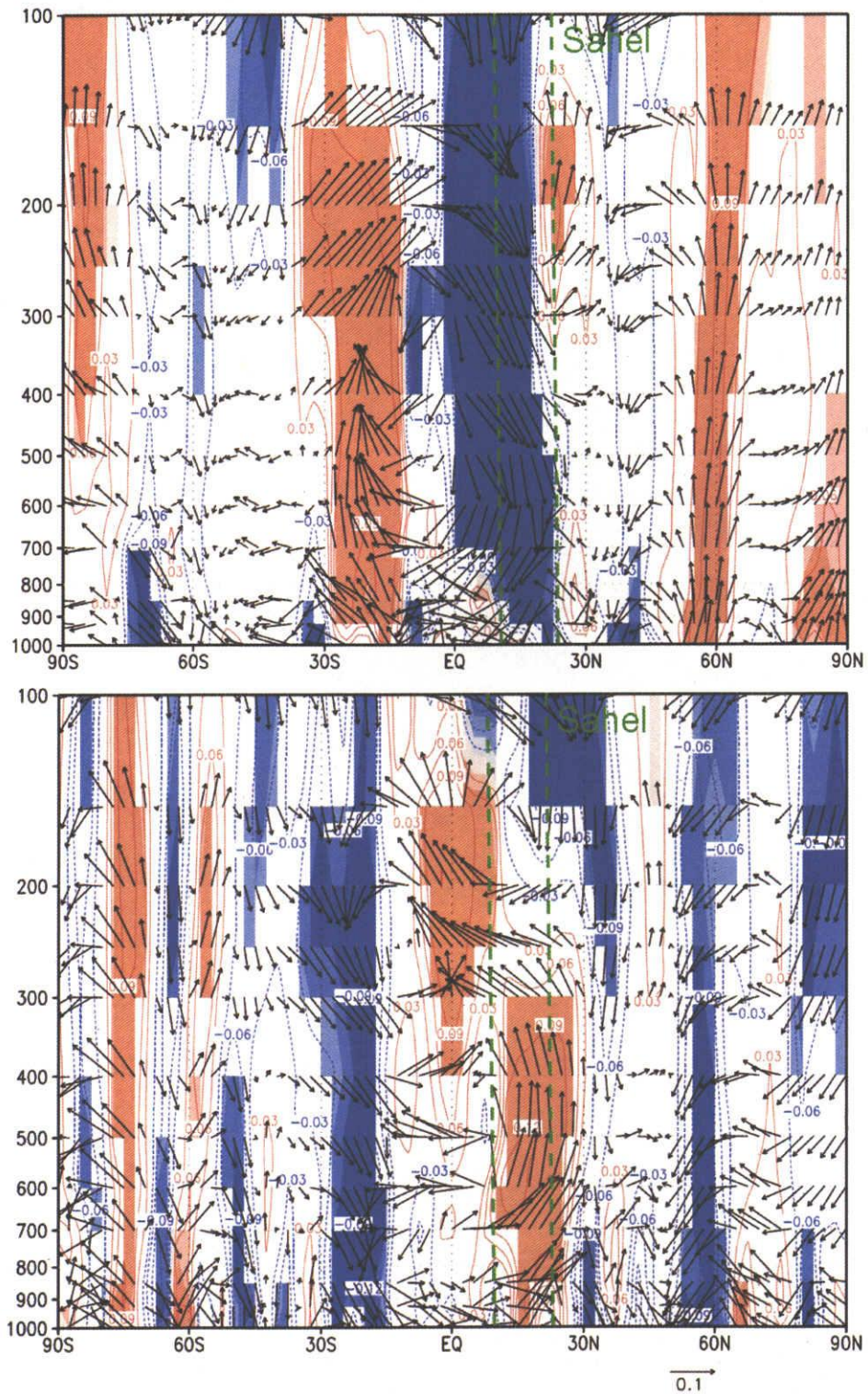


Fig.16 Vertical cross section of the trends of the meridional and vertical winds averaged from 20° W through 50° E before 1984 (top) and after 1984 (bottom). Reddish (Bluish) color indicates northward and upward (southward and downward) trends and contour intervals are 0.03. Shaded areas are the same as Fig.3.

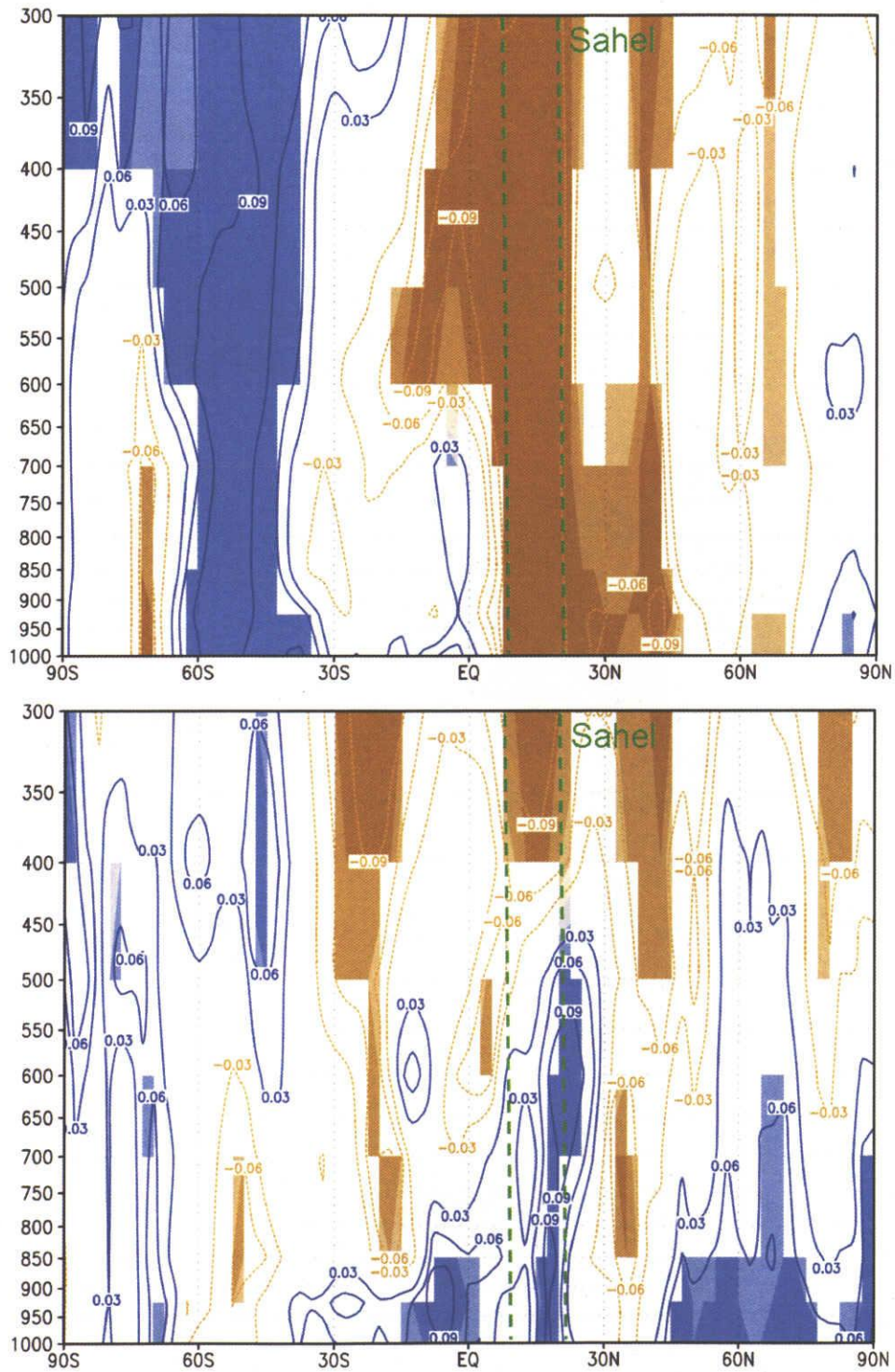


Fig.17 Vertical cross section of the trends of the specific humidity averaged from 20° W through 50° E before 1984 (top) and after 1984 (bottom). Bluish (Brownish) color indicates wet (dry) trends and contour intervals are 0.03. Shaded areas are the same as Fig.3.

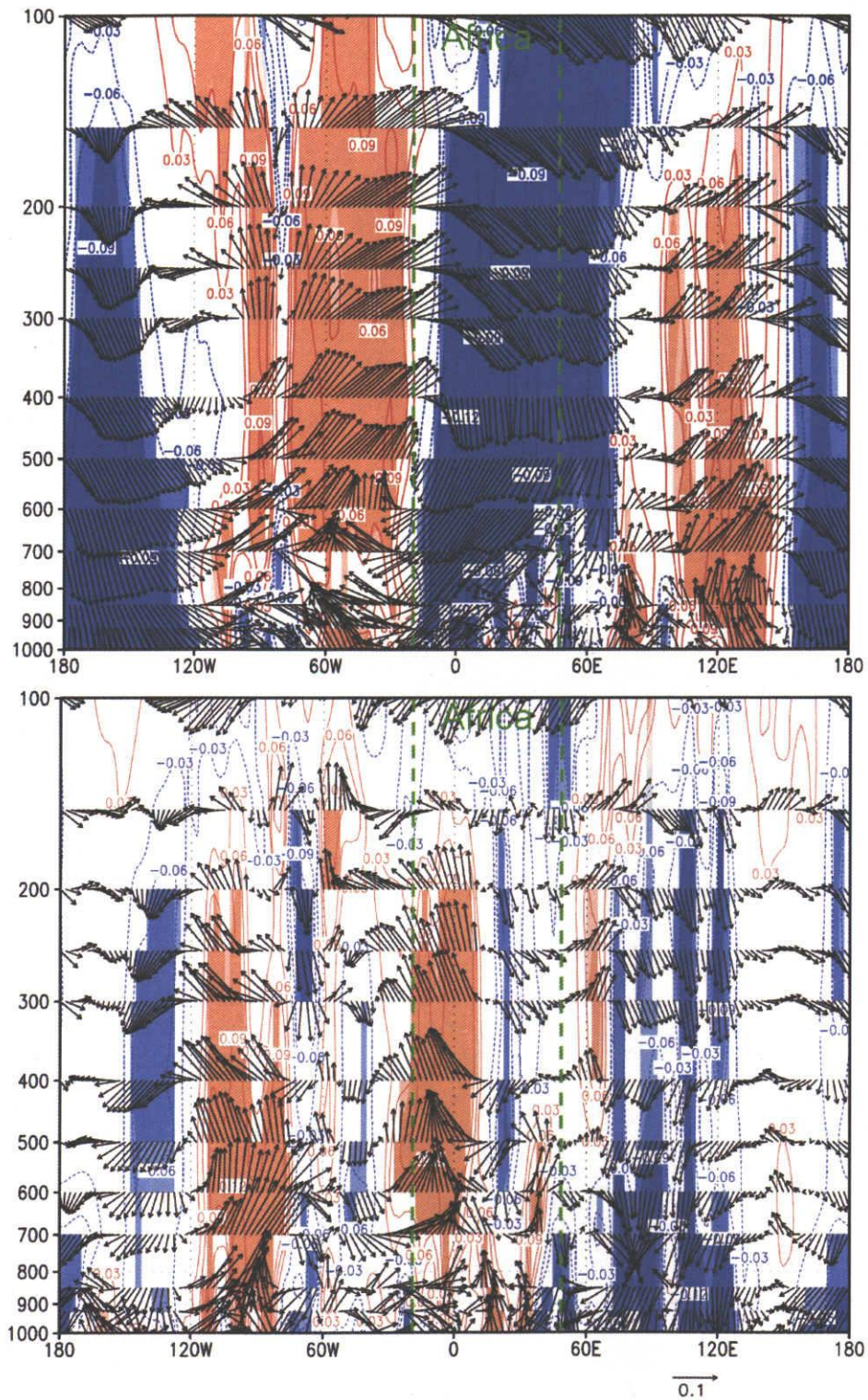


Fig.18 As in Fig.16 except for the trend of the zonal and vertical winds averaged from equator through  $25^{\circ}\text{N}$  and that reddish (bluish) color indicates eastward and upward (westward and downward) trends.

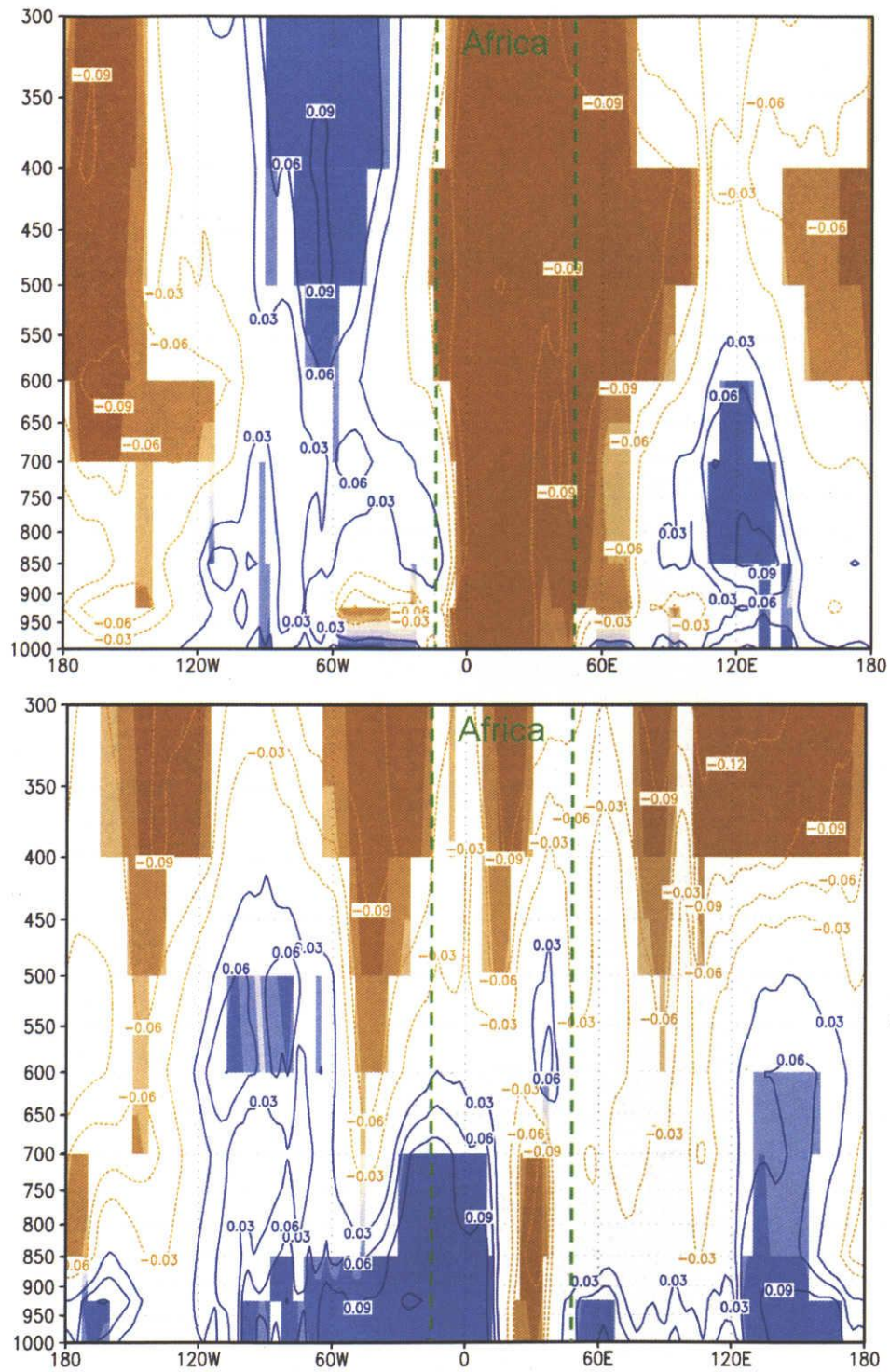


Fig.19 As in Fig.17 except for the trends of the specific humidity averaged from equator through 25° N.

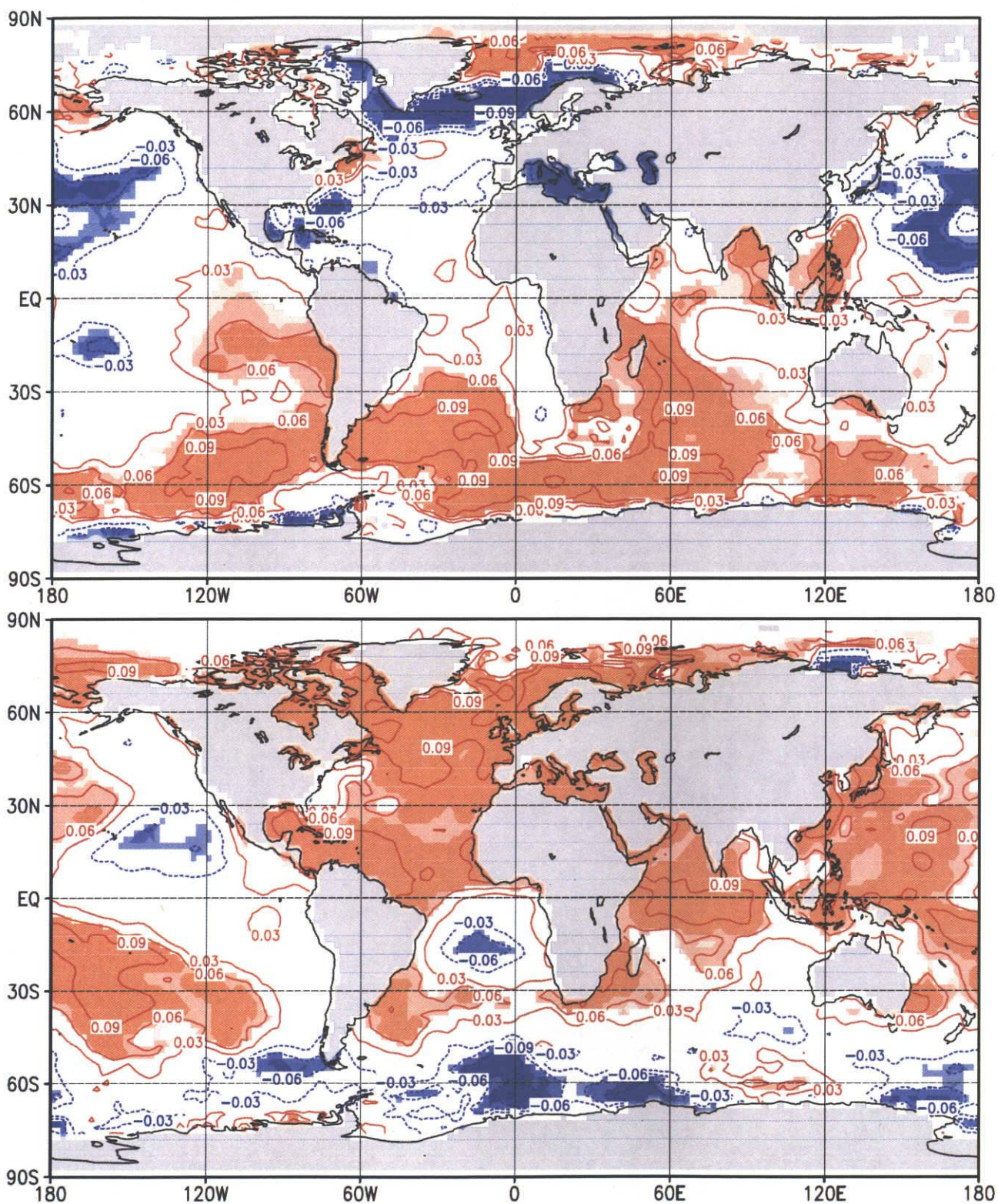


Fig.20 Trends of SST between before 1984 (top) and after 1984 (bottom). Reddish (Bluish) color indicates warming (cooling) trend and contour intervals are 0.03. Shaded areas are the same as Fig.3.

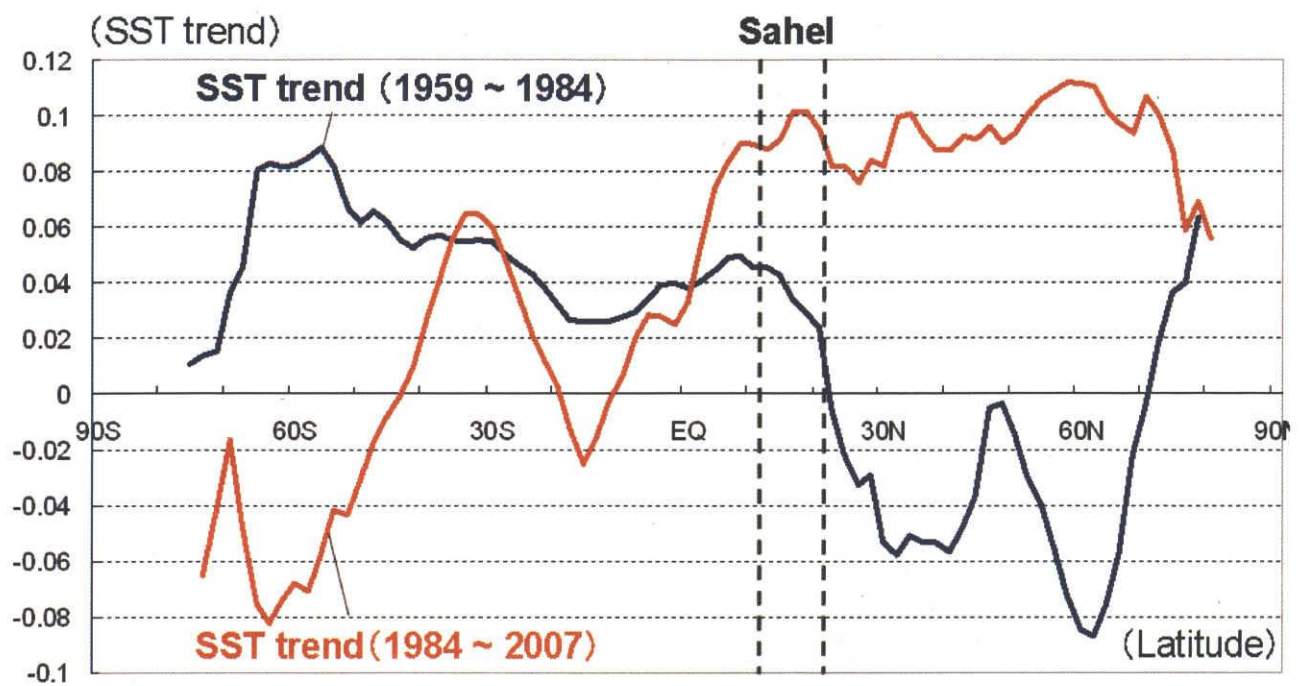


Fig.21 SST trends averaged from 20° W through 50° E. Vertical axis is SST trend and horizontal axis is latitude. Dark blue (Orange) lines depict the trends before (after) 1984.

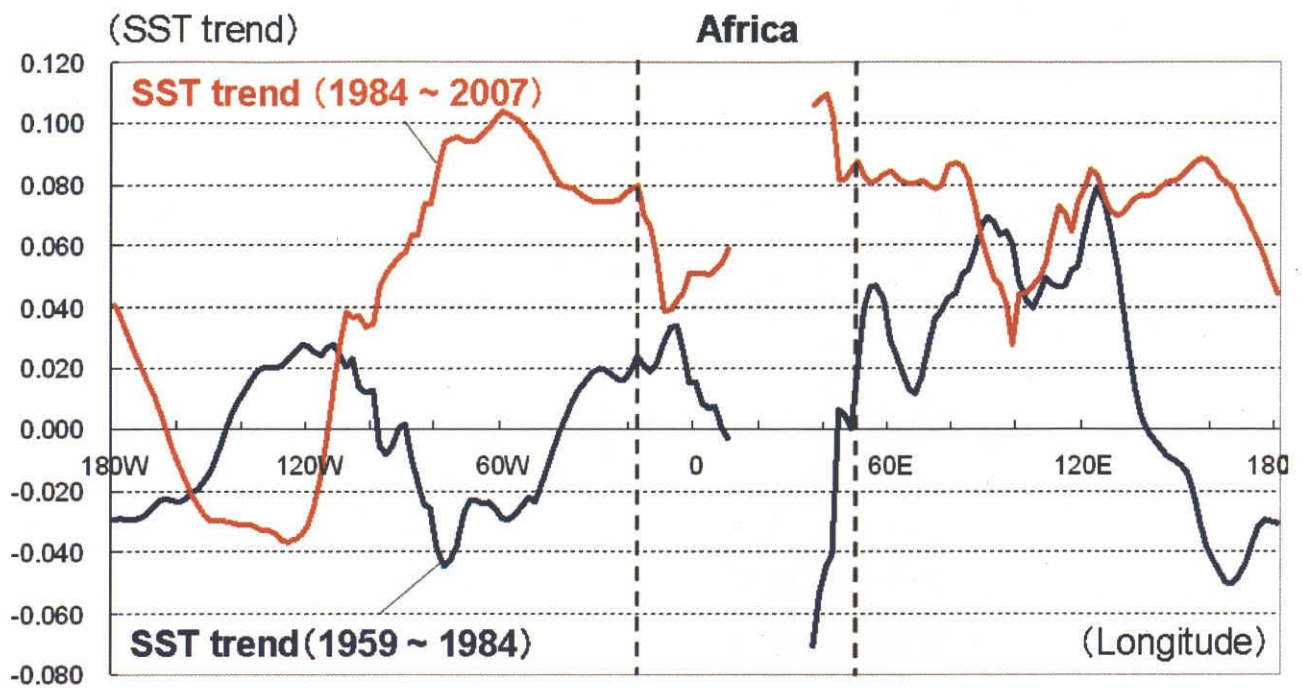


Fig.22 SST trends averaged from equator through 25° N. Vertical axis is SST trend and horizontal axis is longitude. Dark blue (Orange) lines depict the trends before (after) 1984.

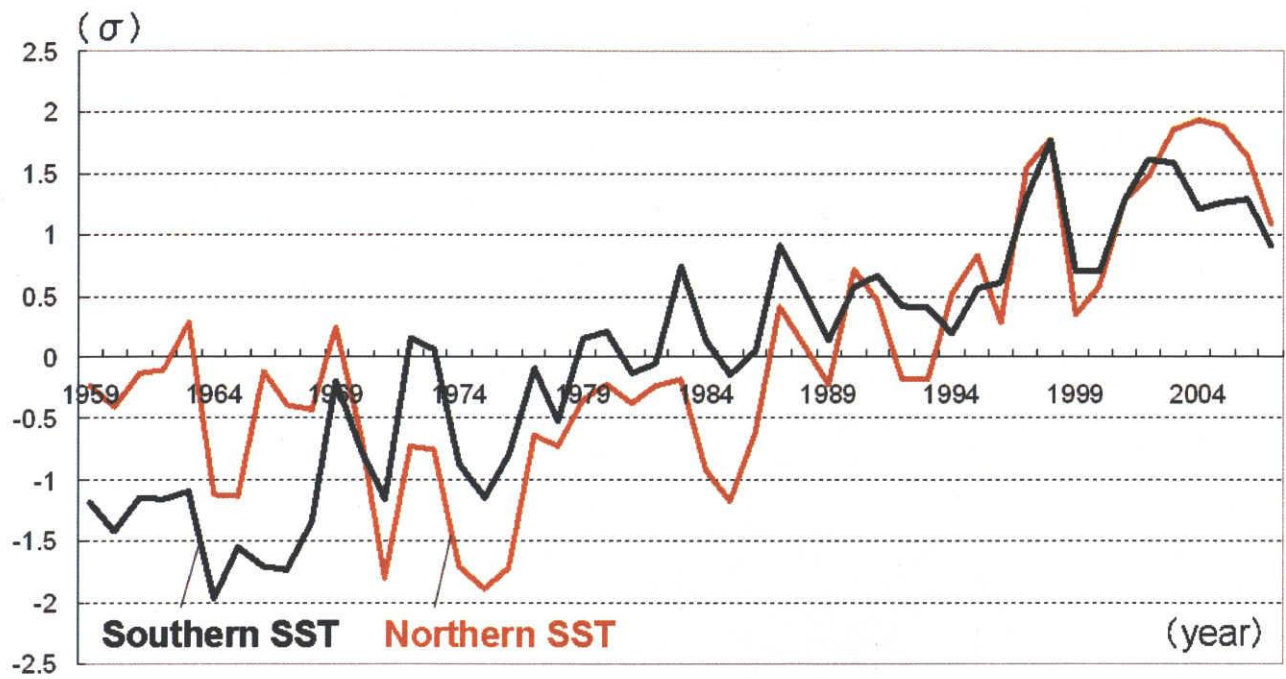


Fig.23 Time series of normalized SST anomalies averaged within northern (orange) and southern (black) hemisphere.

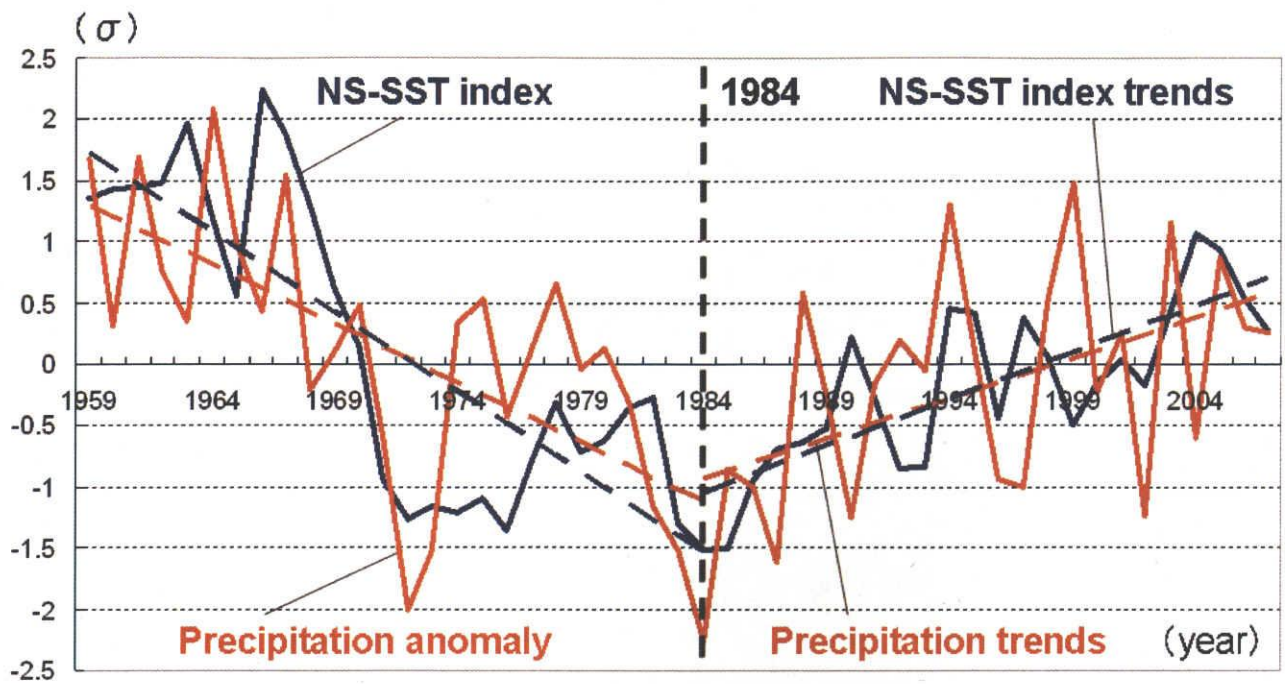


Fig.24 Normalized precipitation anomalies (orange) in Sahel and North-South SST polarity index that is the subtraction of the SST averaged all over the southern hemisphere from the SST averaged all over the northern hemisphere (dark blue), and their linear regression lines before 1984 and after 1984.

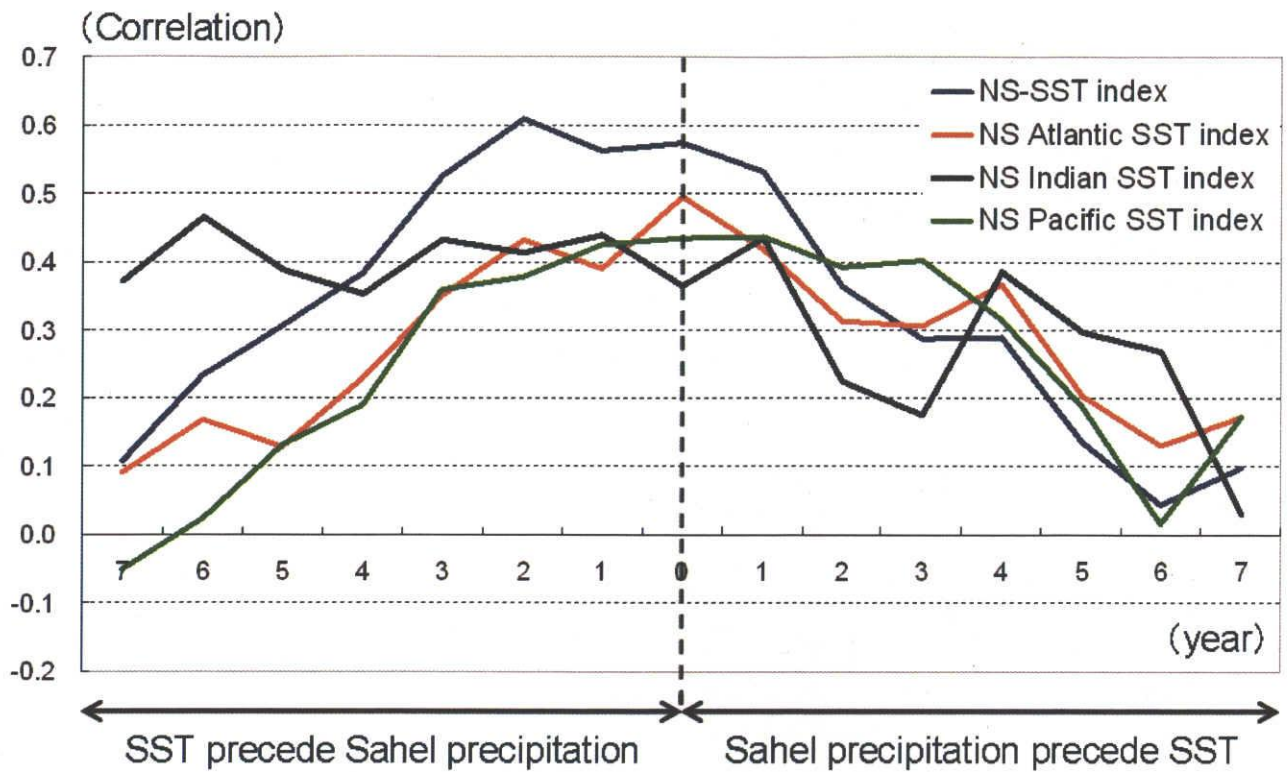


Fig.25 Lag-correlation between Sahel precipitation anomaly and NS-SST polarity index (dark blue), North-South Atlantic SST polarity index (Orange), North-South Indian SST polarity index (black), and North-South Pacific SST polarity index (green).

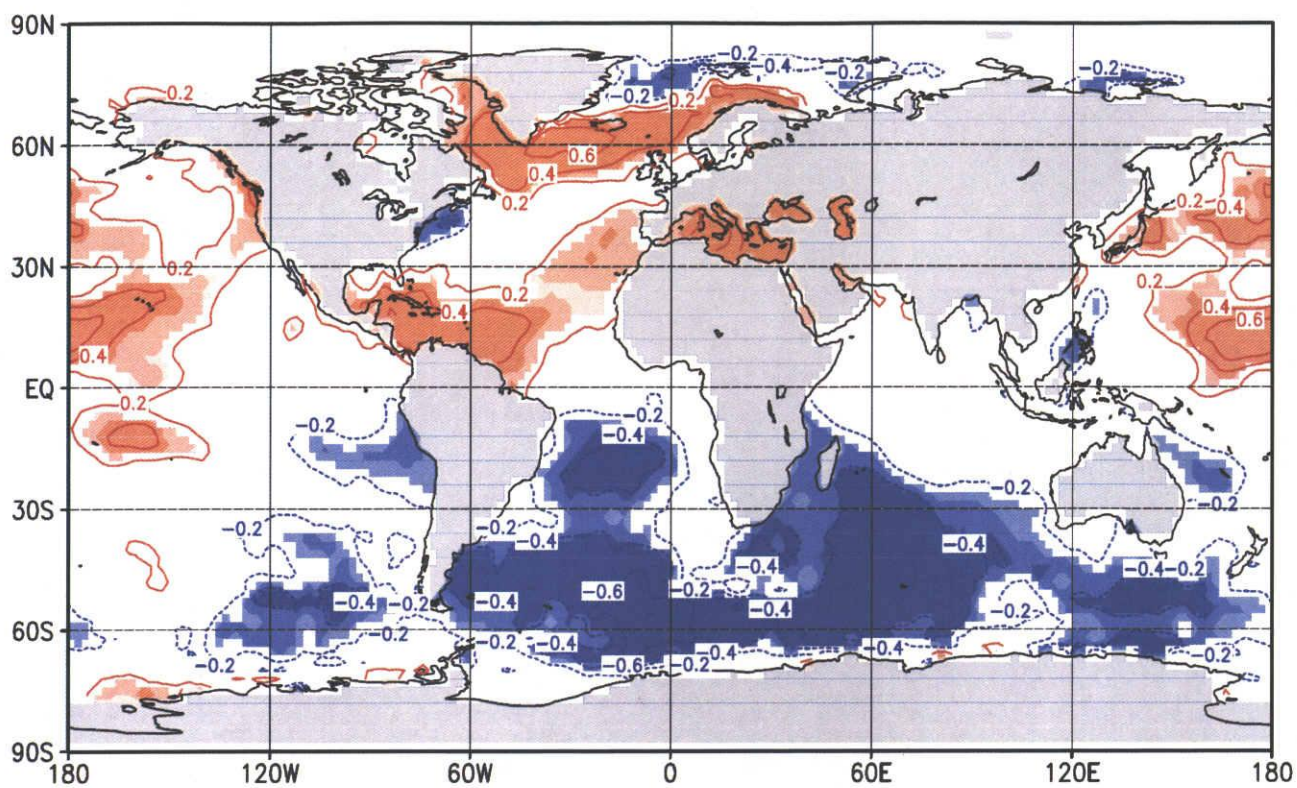


Fig.26 Correlations between the NS-SST index and the global SST for the time lag of 0 year. Reddish (Bluish) color indicates positive (negative) correlations and contour intervals are 0.2. Shaded areas are the same as Fig.3.

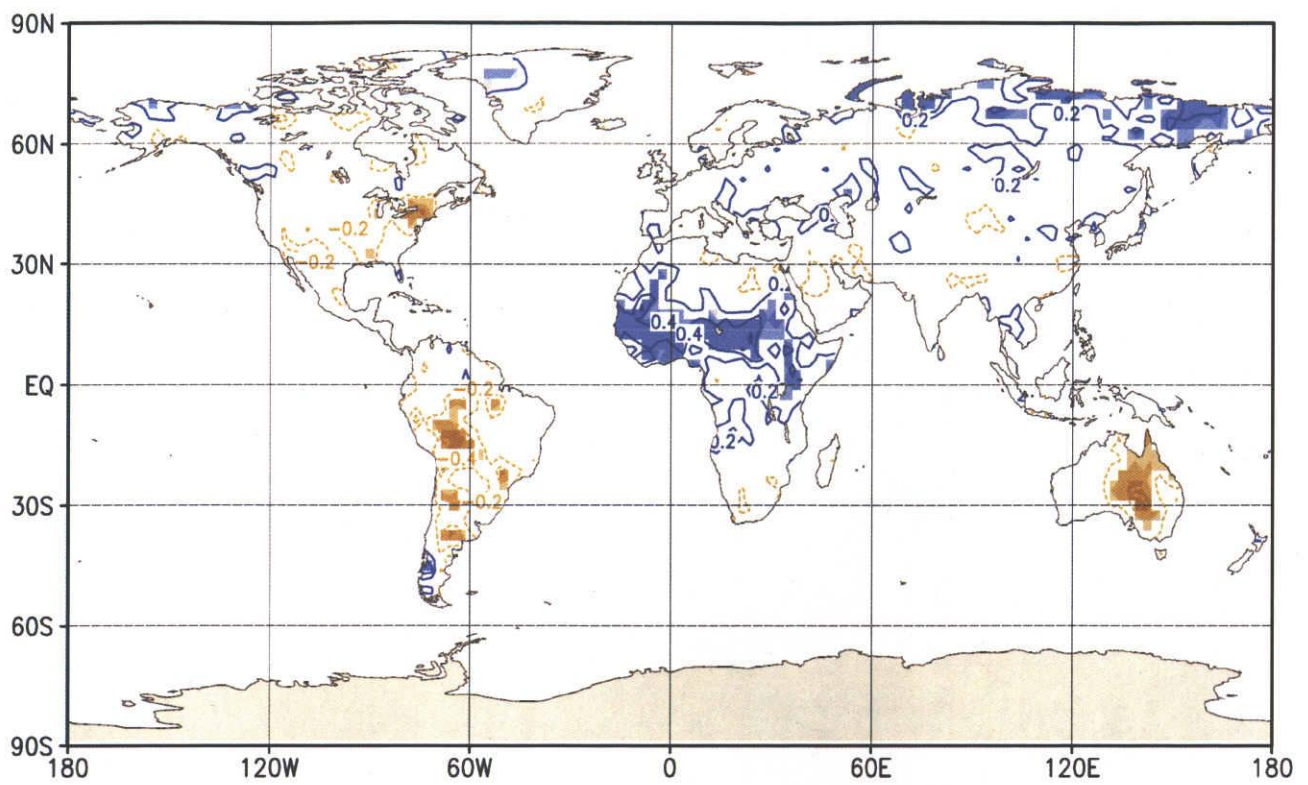


Fig.27 Correlations between the NS-SST index and the normalized precipitation anomalies for the time lag of 0 year. Bluish (Brownish) color indicates positive (negative) correlations and contour intervals are 0.2. Shaded areas are the same as Fig.3.

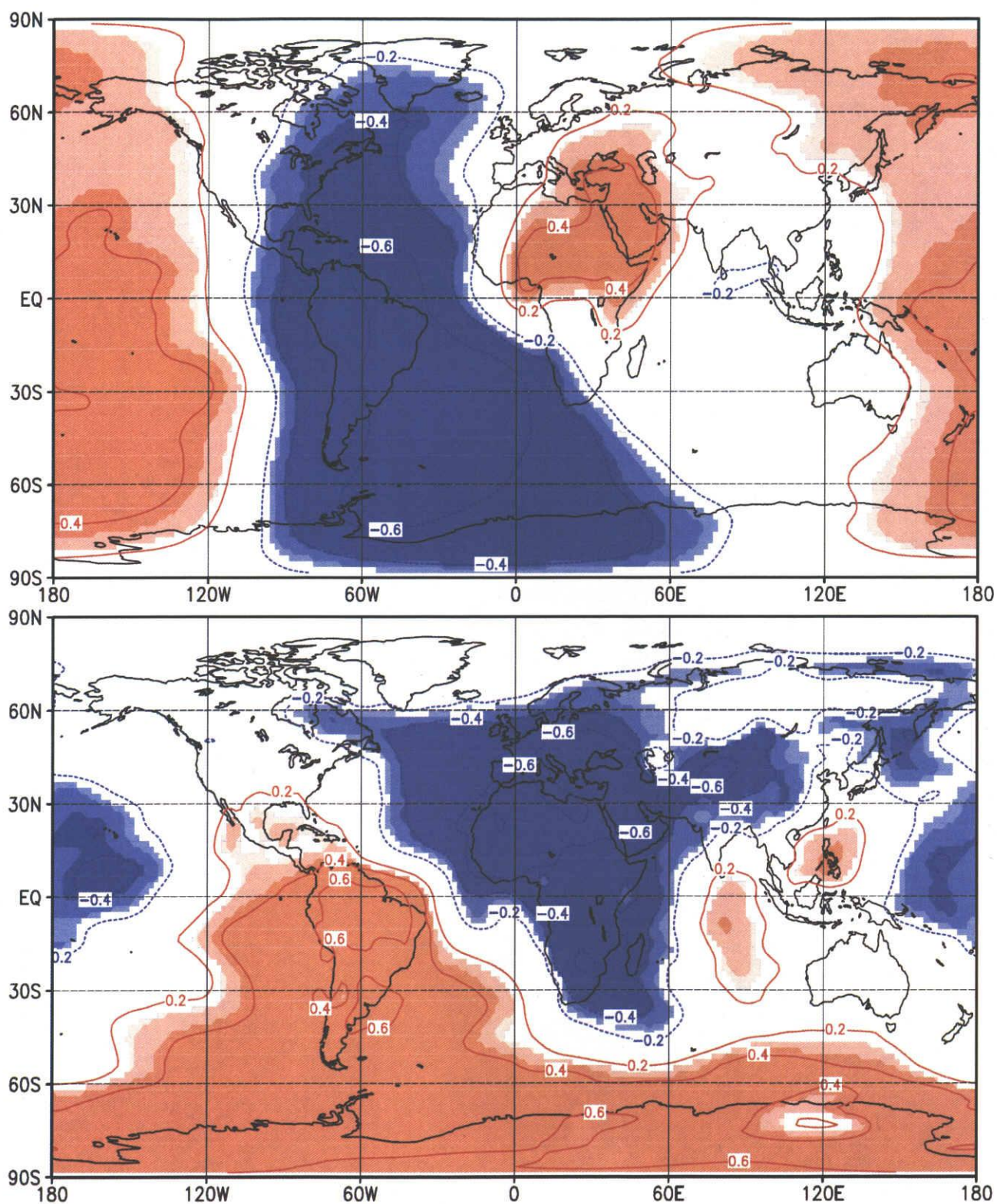


Fig.28 As in Fig.26 except for between the NS-SST index and velocity potential at 0.2101 sigma level (top) and at 0.995 sigma level (bottom).

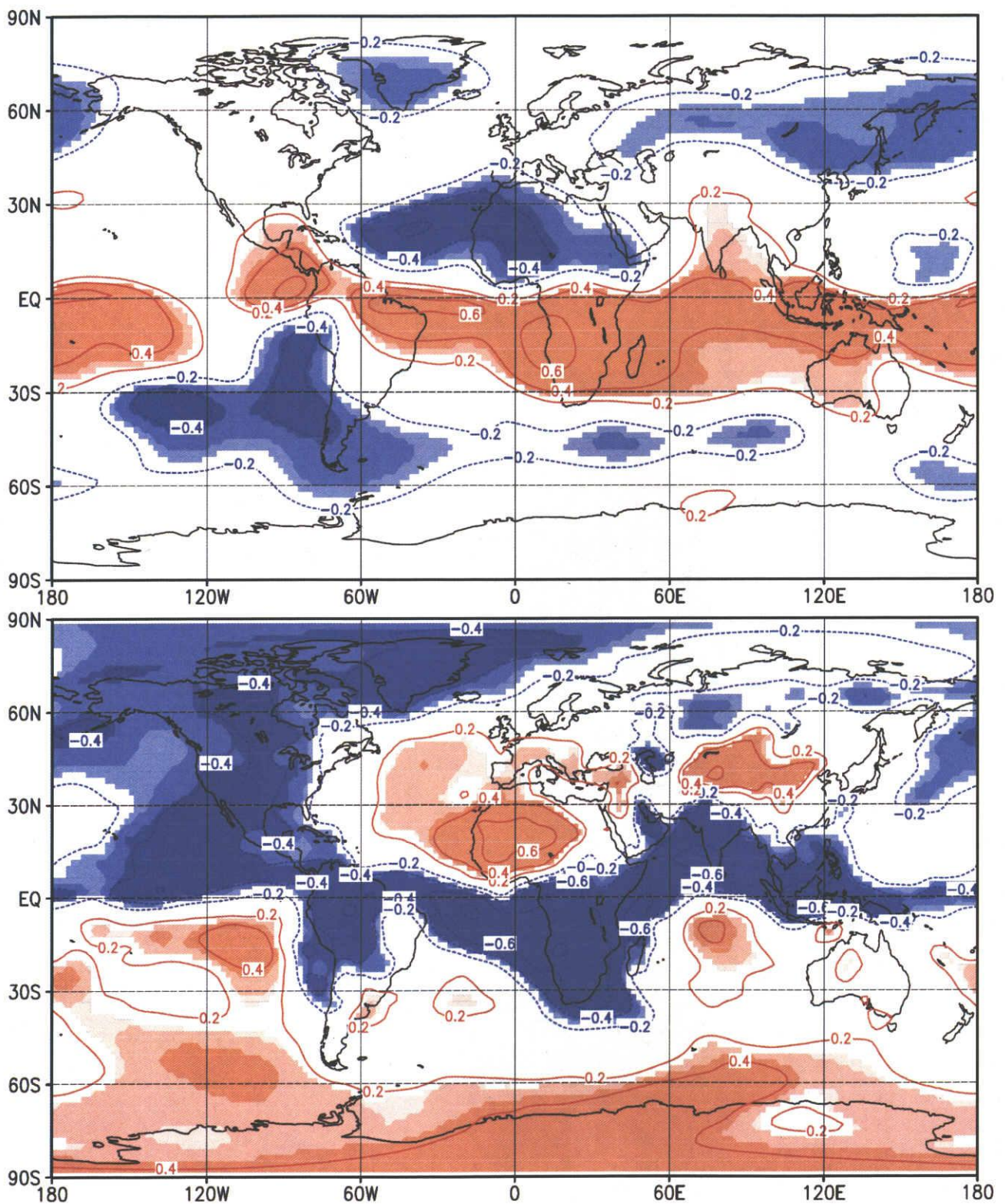


Fig.29 As in Fig.28 except for between the NS-SST index and streamfunction.

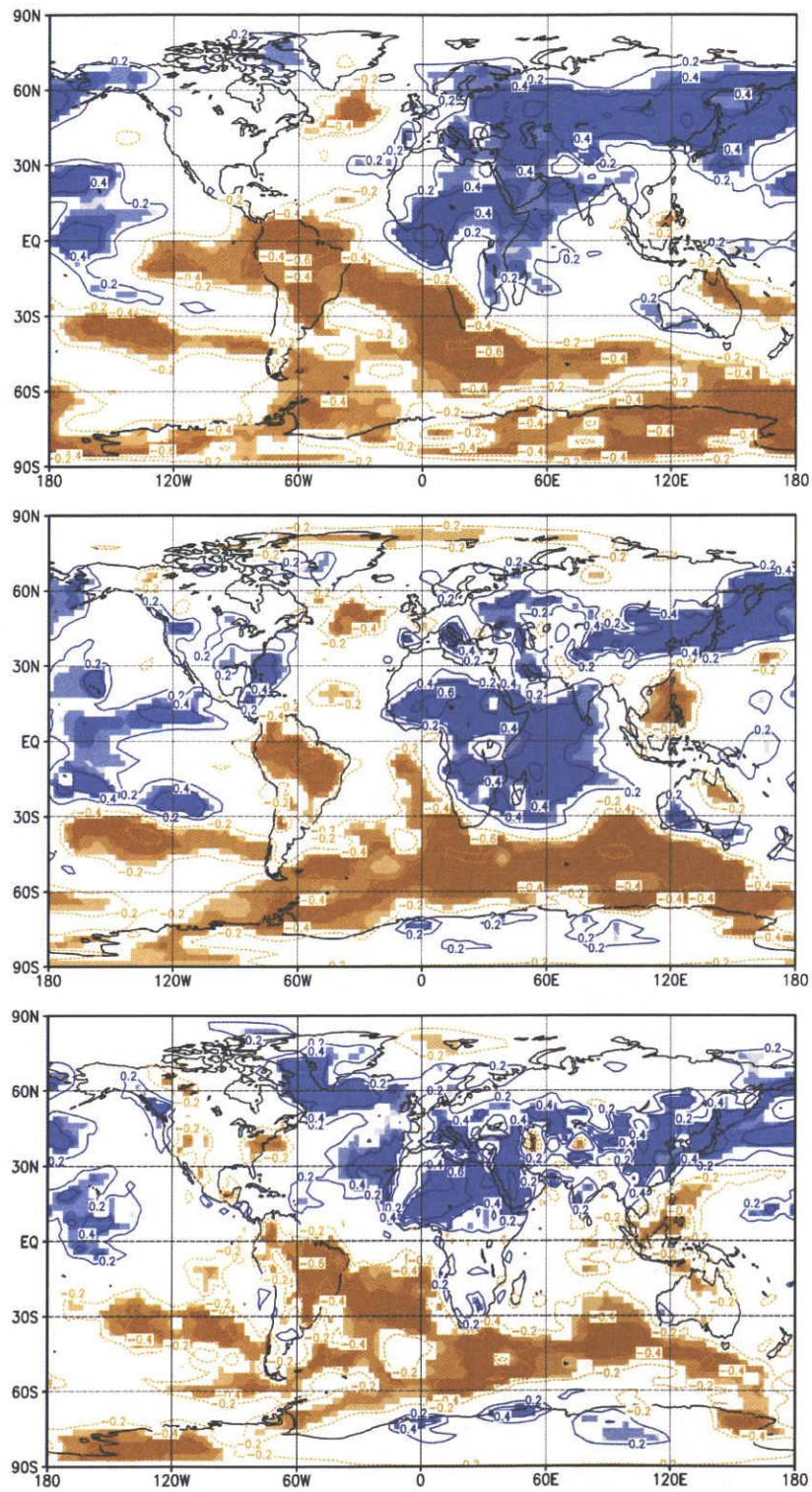


Fig.30 As in Fig.27 except for between the NS-SST index and the specific humidity at 300hPa (top), 600hPa (middle), 1000hPa (bottom) and that bluish (brownish) color indicates positive (negative) correlations.

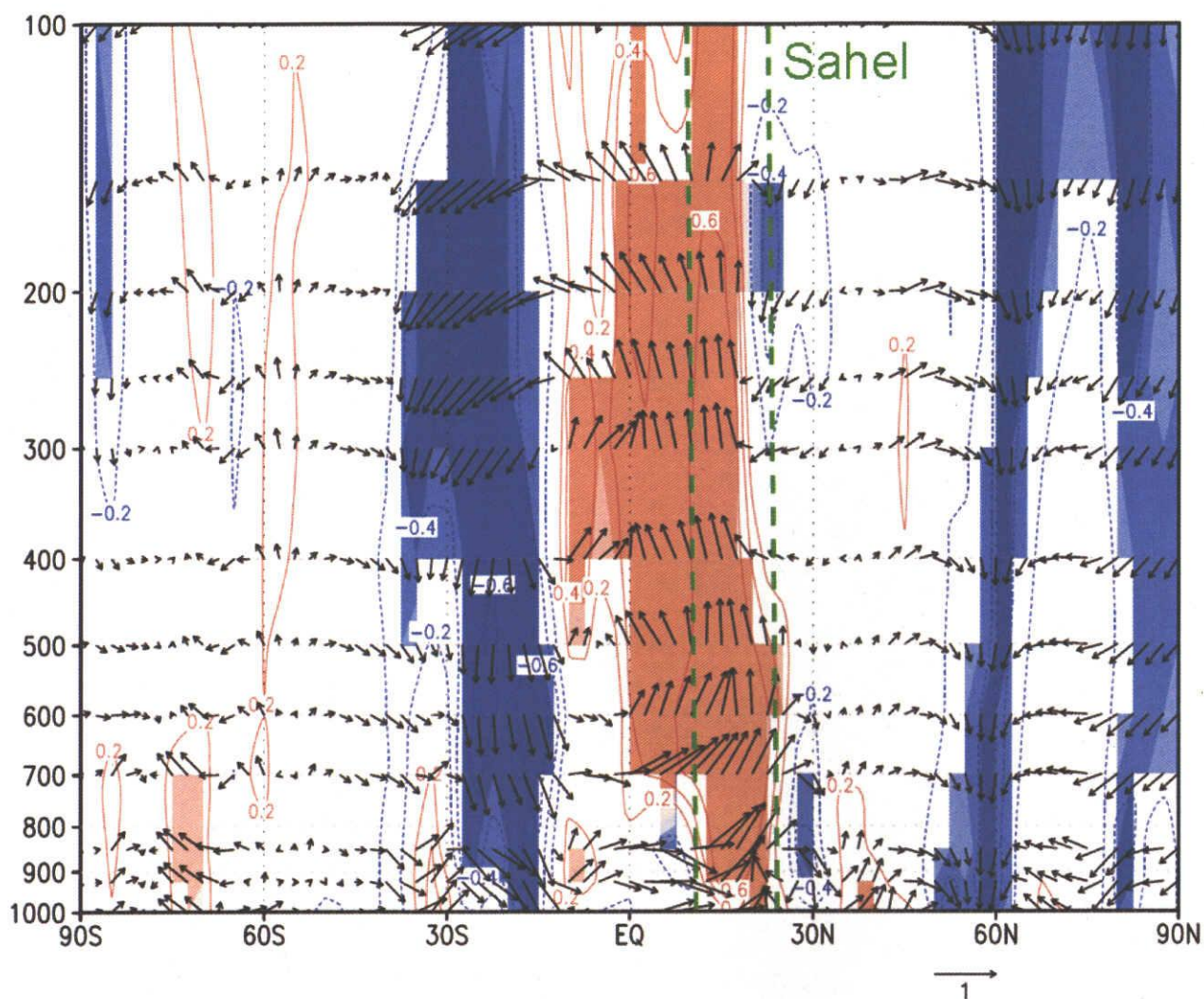


Fig.31 Vertical cross section of the correlations between NS-SST index and the meridional and vertical winds averaged from 20° W through 50° E. Reddish (Bluish) color indicates positive (negative) correlations and contour intervals are 0.03. Shaded areas are the same as Fig.3.

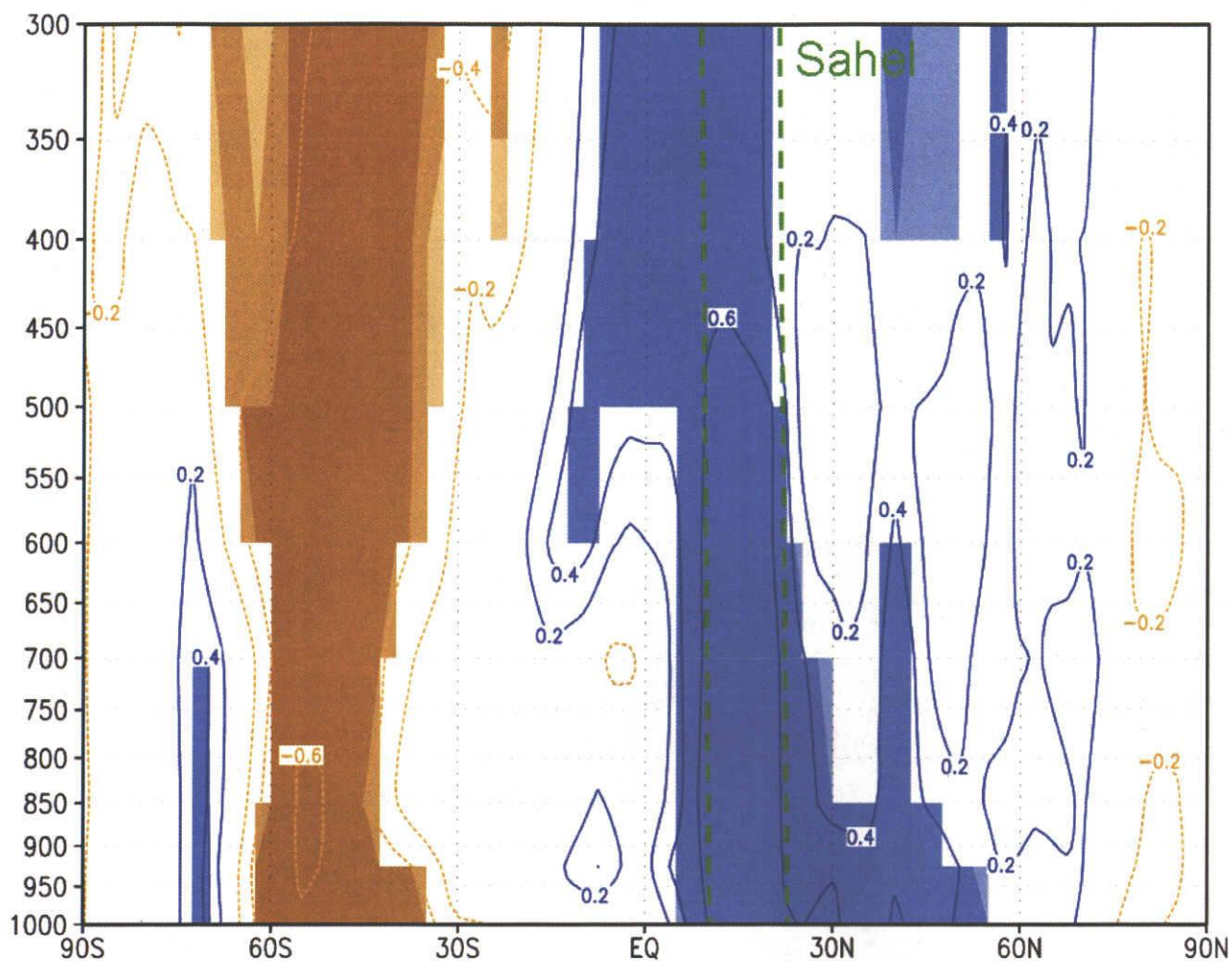


Fig.32 Vertical cross section of the correlations between NS-SST index and the specific humidity averaged from  $20^{\circ}$  W through  $50^{\circ}$  E. Bluish (Brownish) color indicates positive (negative) correlations and contour intervals are 0.03. Shaded areas are the same as Fig.3.

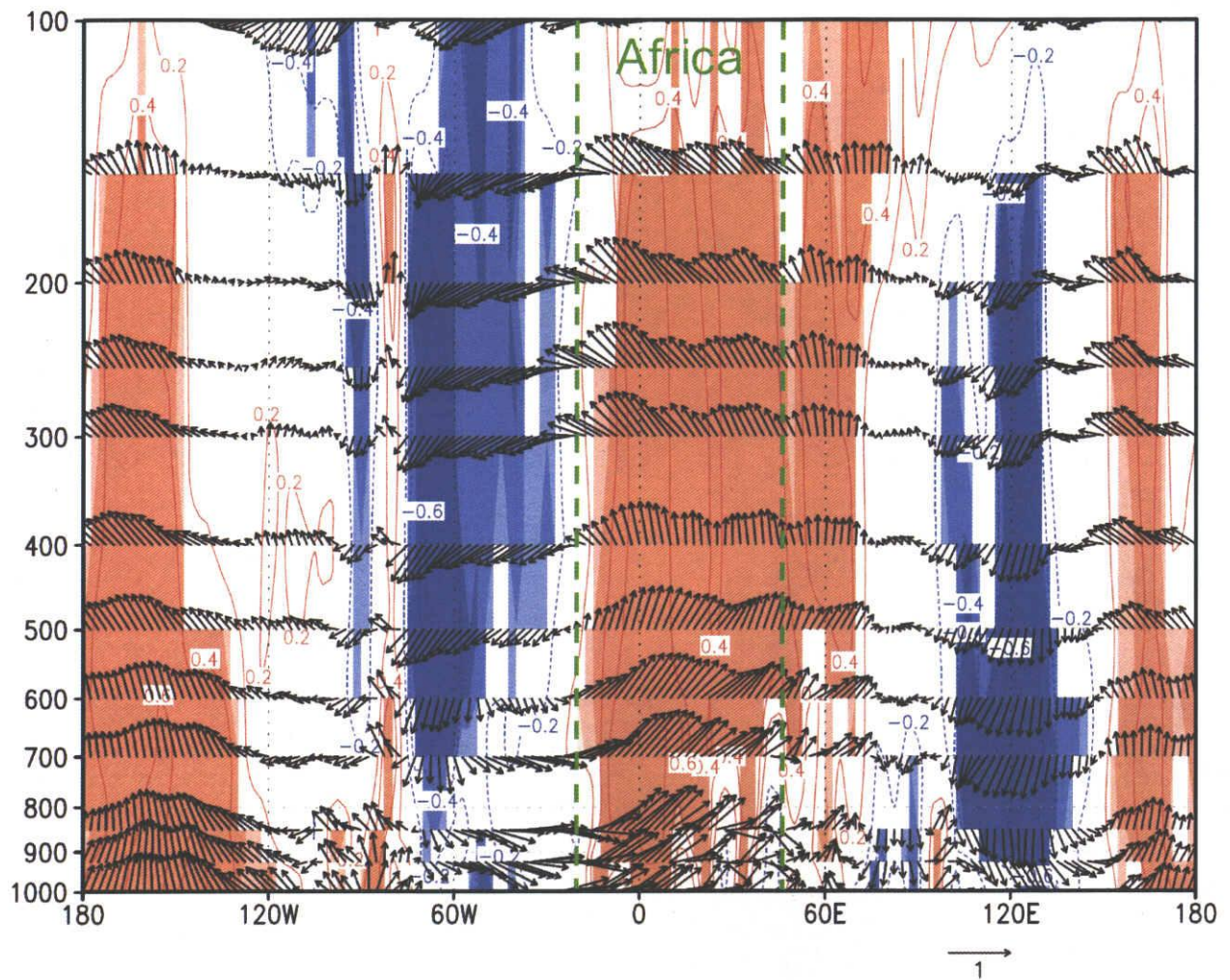


Fig.33 As in Fig.31 except for the zonal and vertical winds averaged from equator through  $25^{\circ}$  N.



Table 1 Lag-correlations between the North-South SST polarity index and Sahel precipitation

Preceding events	Time lag (year)	Correlations
NS-SST index	7	0.11
	6	0.23
	5	0.31
	4	0.38
	3	0.52
	<b>2</b>	<b>0.61</b>
	1	0.56
The same	0	0.57
Sahel precipitation	1	0.53
	2	0.37
	3	0.29
	4	0.29
	5	0.14
	6	0.05
	7	0.10

## Appendix

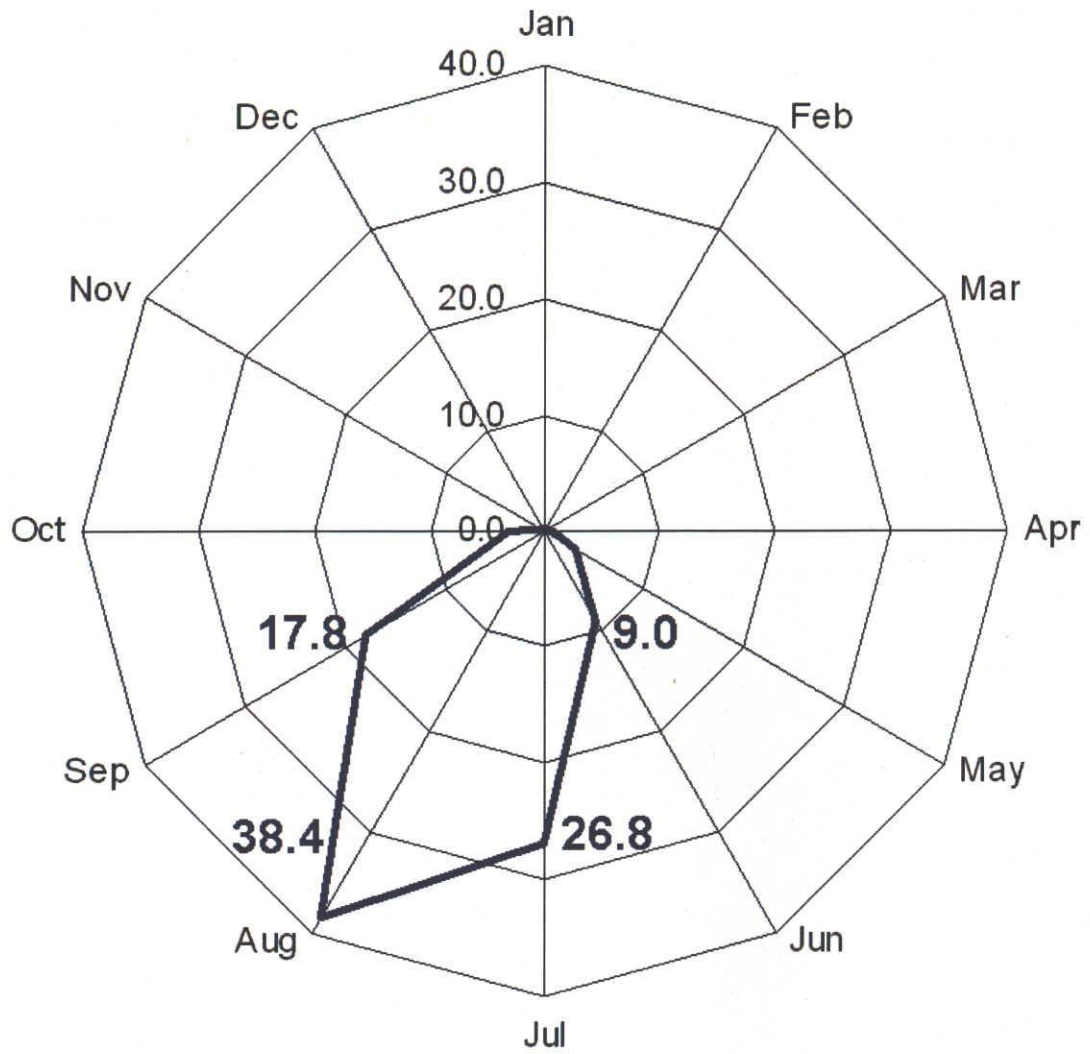


Fig.1A Ratio of monthly precipitation with the annual precipitation averaged from 1959 through 2007.

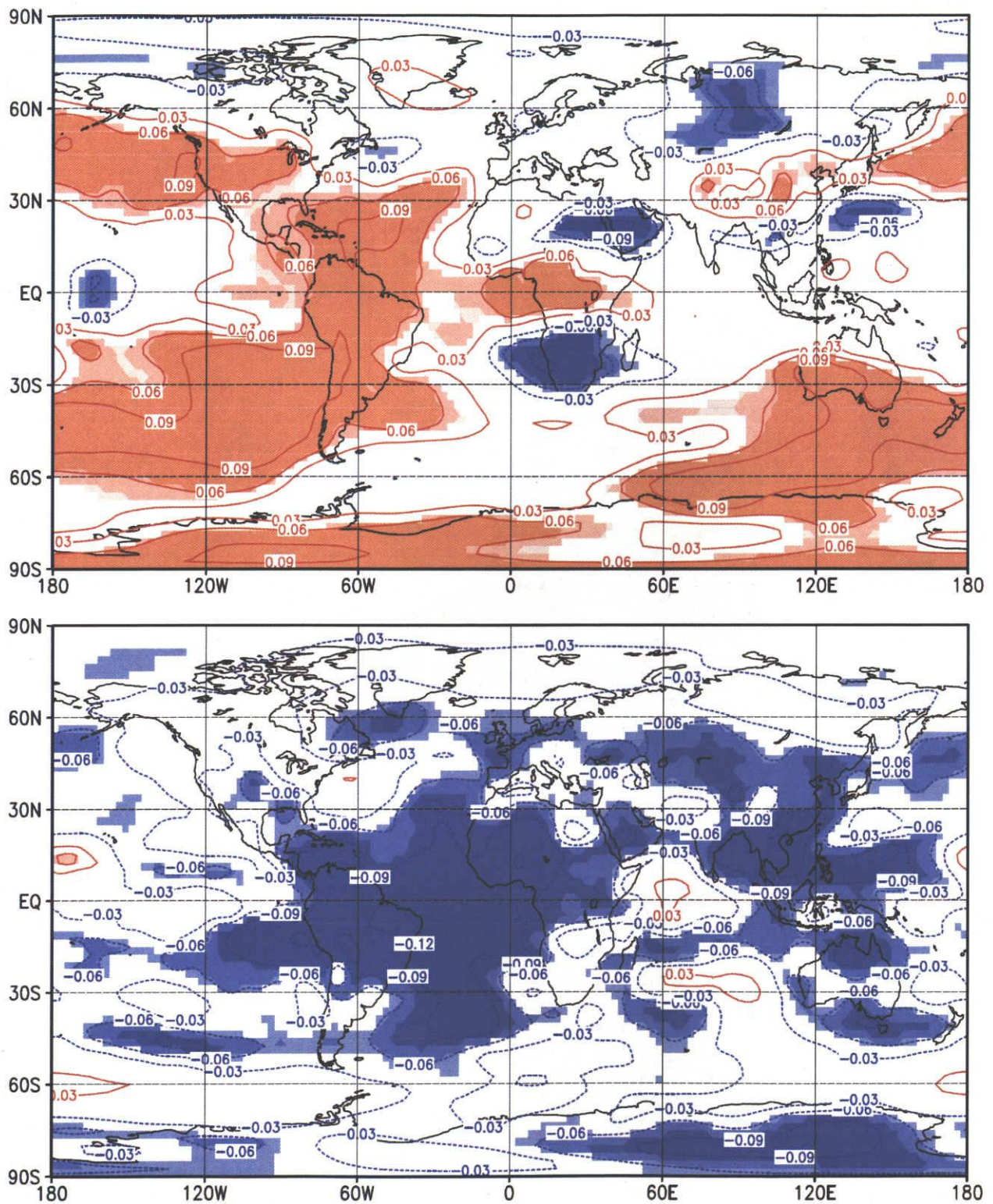


Fig.2A Trends of the atmospheric stability between 200hPa and 600hPa before 1984 (top) and after 1984 (bottom). Reddish (Bluish) color indicates stable (unstable) trends and contour intervals are 0.03. Shaded areas are the same as Fig.3.

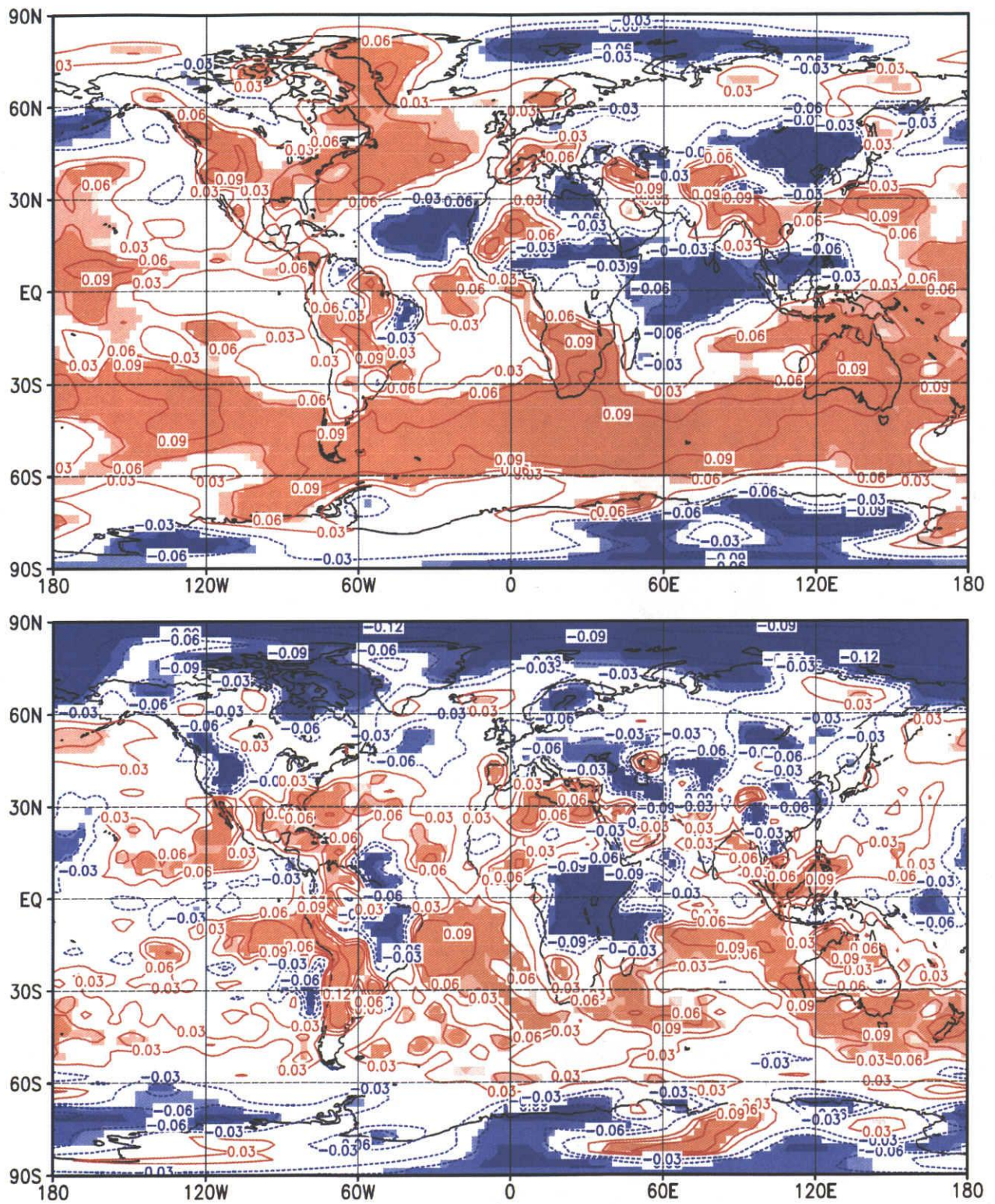


Fig.3A As in Fig.2A except for between 600hPa and 1000hPa.